行政院國家科學委員會專題研究計畫 成果報告

使用多段曲線擬合方法實現CMOS電流模式函數
研究成果報告(精簡版)

計 畫 類 別 ：個別型
計 畫 編 號 ：NSC 100-2221-E-216-033-
執 行 期 間 ：100年08月01日至101年07月31日
執 行 單 位 ：中華大學電子工程學系

計 畫 主 持 人：林國珍

計畫參與人員：博士班研究生-兼任助理人員：鄭智仁

報 告 附 件 ：出席國際會議研究心得報告及發表論文

公 開 資 訊 ：本計畫可公開查詢

中 華 民 國 101年10月27日

中 文 摘 要 ： 由於愈來愈多的類比電路採用 CMOS 電流模式來發展，輸入動態範圍一直都是電流模式優於電壓模式的項目。然而為了解決更多的問題，輸入動態範圍也被要求提高，因此如何設計電路讓輸入動態範圍提昇將是一個重要的議題。

本研究計畫將一函數在所要求的輸入動態範圍內採用多段曲線擬合的方法來提升精確度，也就是說在一個固定誤差範圍內，增加輸入動態範圍。我們將預先設定範圍之函數依照曲率的不同作分段，使用 Divide-and-Conquer（分治法）以二元樹架構來做分割。分割後的每一分段是以 Taylor 展開式的二次多項式來擬合，兼顧電路精簡化及擬合精準度。

控制如何分段的電路是參考差動放大器為基礎的電壓比較器，並經修改後成為電流模式比較器，以作為分割線段的依據。每一分段的二次多項式均含有控制界面，受電流模式比較器的控制。二次多項式電路的構成是採用 PMOS 與 NMOS 的背對背電路架構，再根據不同的 ax2 + bx + c 二次多項式係數，改變 Mirror 比例及定電流值所形成，最後將各段之電流輸出合起來產生所要函數的電流輸出。

在本研究計畫已將電路下線製作成晶片，Post-Simulation 所得結果與模擬結果及理想函數作比較來驗證成果。

中文關鍵詞： CMOS 電流模式電路、輸入動態範圍、電流模式比較器、差動放大器、分段函數、二次多項式電路、曲線擬合。

英 文 摘 要 ： A significant increase in the use of CMOS current-mode technology for the realization of analog circuits has been observed. In most applications, high accuracy result and large input dynamic range are required. Therefore, how to design a large input dynamic-range circuit becomes an important issue.

In this project, we will use a multi-segments method to fit a function with a large input dynamic range and high accuracy result. We use a divide-and-conquer algorithm, according to the curvature of a function, to construct a binary tree. In each divided segment, we approximate the segmented function using a second-order polynomial which is suited for simple circuit and good for accurate result.

We implement a current-mode comparator, using a modified voltage-mode comparator based on a

differential amplifier, to divide a function. The segmented function is constructed by a pair of PMOS and NMOS. We can properly use the scale of current-mirror and add a current source to make a second-order polynomial form of ax2 + bx + c.

In this project, we design and implement chips to verify a large input dynamic range and a high accuracy result. We also compare measurement results with corresponding simulations.

英文關鍵詞： CMOS current-mode circuit, input dynamic range, current-mode comparator, differential amplifier, segmented function, quadratic circuit, curve fitting.

行政院國家科學委員會補助專題研究計畫 □期中進度報告 ■期末報告

（使用多段曲線擬合方法實現CMOS 電流模式函數）

計畫類別：■個別型計畫　□整合型計畫
計畫編號：NSC 100 － 2221 － E － 216 － 033 －
執行期間：　100 年 08 月　01 日至　101 年 07 月　31 日

執行機構及系所：中華大學電子工程學系

計畫主持人：林國珍
共同主持人：
計畫參與人員：鄭智仁

本計畫除繳交成果報告外，另須繳交以下出國報告：
□赴國外移地研究心得報告
□赴大陸地區移地研究心得報告
■出席國際學術會議心得報告及發表之論文
□國際合作研究計畫國外研究報告

處理方式：除列管計畫及下列情形者外，得立即公開查詢
□涉及專利或其他智慧財產權，□一年□二年後可公開查詢

中　華　民　國　101 年　10 月　27 日

中文摘要

由於愈來愈多的類比電路採用 CMOS 電流模式來發展，輸入動態範圍一直都是電流模式優於電壓模式的項目。然而為了解決更多的問題，輸入動態範圍也被要求提高，因此如何設計電路讓輸入動態範圍提昇將是一個重要的議題。

本研究計畫將一函數在所要求的輸入動態範圍內採用多段曲線擬合的方法來提升精確度，也就是說在一個固定誤差範圍內，增加輸入動態範圍。我們將預先設定範圍之函數依照曲率的不同作分段，使用 Divide-and-Conquer (分治法)以二元樹架構來做分割。分割後的每一分段是以 Taylor 展開式的二次多項式來擬合，兼顧電路精簡化及擬合精準度。

控制如何分段的電路是參考差動放大器為基礎的電壓比較器，並經修改後成為電流模式比較器，以作為分割線段的依據。每一分段的二次多項式均含有控制界面，受電流模式比較器的控制。二次多項式電路的構成是採用 PMOS 與 NMOS 的背對背電路架構，再根據不同的 $ax^2 + bx + c$ 二次多項式係數，改變 Mirror 比例及定電流值所形成，最後將各段之電流輸出合起來產生所要函數的電流輸出。

在本研究計畫已將電路下線製作成晶片，Post-Simulation 所得結果與模擬結果及理想函數作比較來驗證成果。

關鍵詞：CMOS 電流模式電路、輸入動態範圍、電流模式比較器、差動放大器、分段函數、二次多項式電路、曲線擬合。

Abstract

A significant increase in the use of CMOS current-mode technology for the realization of analog circuits has been observed. In most applications, high accuracy result and large input dynamic range are required. Therefore, how to design a large input dynamic-range circuit becomes an important issue.

In this project, we will use a multi-segments method to fit a function with a large input dynamic range and high accuracy result. We use a divide-and-conquer algorithm, according to the curvature of a function, to construct a binary tree. In each divided segment, we approximate the segmented function using a second-order polynomial which is suited for simple circuit and good for accurate result.

We implement a current-mode comparator, using a modified voltage-mode comparator based on a differential amplifier, to divide a function. The segmented function is constructed by a pair of PMOS and NMOS. We can properly use the scale of current-mirror and add a current source to make a second-order polynomial form of $ax^2 + bx + c$.

In this project, we design and implement chips to verify a large input dynamic range and a high accuracy result. We also compare measurement results with corresponding simulations.

Keywords: CMOS current-mode circuit, input dynamic range, current-mode comparator, differential amplifier, segmented function, quadratic circuit, curve fitting.

目錄

一、前言

輸入動態範圍一直都是 CMOS 電流模式優於 CMOS 電壓模式的項目。然而為了解決更多的問題，輸入動態範圍也一再被提升，因此如何設計電路讓輸入動態範圍擴大是一個重要的議題。

本研究計畫採用分割的方法將一函數分成多段二次多項式函數，控制分割的方法及電路為主要的研究對象。我們將控制電路分成兩種方法來實現，一為 CMOS 差動比較電路，一為 CMOS 電流比較電路。最後整體電路經由 HSPICE 模擬及晶片製作所量測結果做比較以保證電路之可行性。

二、研究目的

本研究計畫希望使用分段的方式將一複雜的函數分成數段，再將每段使用二次多項式 Taylor 展開式來趨近，以達到輸入電流之動態範圍大幅提升。例如要發展一個 exp(x)的電路功能，可以將 exp(x)利用 Taylor 展開式轉換為 n 段的二次多項式來趨近，其中第 k 段可以表示成 $a_k x^2 + b_k x + c_k$。因此，本研究最後可以獲得控制分段的電路及 n 段二次多項式電路來實現一複雜函數的功能，可以大幅改進類比電路之應用範疇及執行效率，例如應用於可變增益放大器(Variable Gain Amplifier)電路發展，可以不需串聯多級電路即可提升線性度；而應用於 LCD 控制電路、FUZZY 控制電路及複雜算術計算電路的發展，均可降低功率消耗及提升動態輸入電流範圍。

三、文獻探討

近二十年來，電流模式類比電路已經漸漸地在類比功能的應用中出現。透過電壓模式信號處理與電流模式的信號處理的結合，可以很明顯地獲得系統性能的提升優勢[1]。現今電流模式的類比信號處理愈來愈成熟，有多種應用系統使用此技術如[1-11]。由於很多潛在的優點 [7, 8, 9], 電流模式電路獲得相當多的注意。與電壓模式電路相比較，電流模式電路擁有以下的潛在的優點：

1. 更高的頻寬能力：雙極電晶體(BJT)和金氧半場效電晶體(MOS)兩個都是電流輸出裝置，以電晶體做為促成均一增益頻寬(fT)之電流放大器。電流模式的關鍵性特徵是在更高的頻率下，雜散電容可以有效地當成增益的元件[10],而電壓模式電路則被限制。

2. 高操作速度：積體電路技術的尺寸縮小導致寄生電容成為電路快慢的因素。因此電流模式電路能在電路內部的節點取得低阻抗和低電壓振幅達到高操作速度。

3. 算術計算的低電路複雜性：在電流模式下，加法和減法的計算可以直接透過在一個結點的連接來執行。再使用電流模式的電流鏡架構可以輕易地處理信號的反向、總和及比例大小等基本功能，而這些基本功能電壓模式就難以處理。很明顯地，電流模式擁有低的電路複雜性和低的功率消耗。

4. 更大的操作動態範圍：當 IC 製程技術愈來愈縮小，為了保證元件可靠性，電源的電壓必須降低。降低的電源電壓導致降低了電壓模式的動態範圍。解決這個問題顯然可從電壓模式改變為電流模式，可以避免電源電壓的限制[11]。

以 CMOS 為主流之 IC 設計及製程而言，MOS 在飽和狀態下，電流與電壓平方的關係成為電流模式的基礎。相關的平方電路及平方根電路已經漸漸地出現在類比功能的應用中[6, 12, 13, 15, 17-21]。其中，最著名的是 MOS Translinear Principle 或稱為 Quadratic-translinear Principle 的提出

及應用[15, 17, 19, 21]，但是這些應用還是受限於平方及平方根的特性。

過去我們利用一個精簡的平方電路架構[22]作為基礎，使用二次多項式 Taylor 展開式來趨近較複雜的函數電路，以精簡的電路實現特殊及較為複雜的功能應用[1-5]。由於 Taylor 展開式的 truncation error 及平方電路的限制，輸入電流之動態範圍在誤差的考量下無法有效及大幅的提升。

四、研究方法

對於一非線性及二次多項式函數或一複雜函數 (例如 EXP(x))，我們可以將一較大的輸入動態範圍區間分成 n 段，每一段均使用二次多項式來表示。以下就控制分段電路之設計、二次多項式電路設計、整合電路設計、模擬電路結果及晶片製作分別作說明。

1、控制分段電路：

首先介紹以差動放大器作為基礎的傳統電壓模式比較器如圖一[24]，作為電流模式控制分段電路設計之參考。

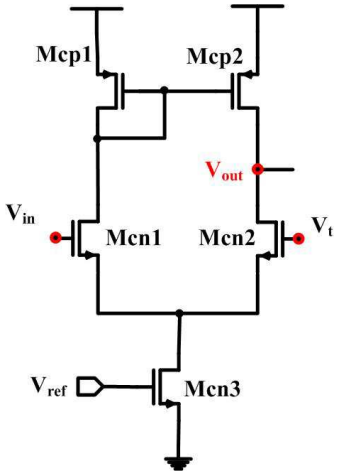

圖一：傳統電壓模式比較器

當 $V_{in} > V_t$，可得 V_{out} 為邏輯 1，否則 V_{out} 為邏輯 0。由於採用電流模式，我們將傳統電壓模式比較器修改成如圖二。

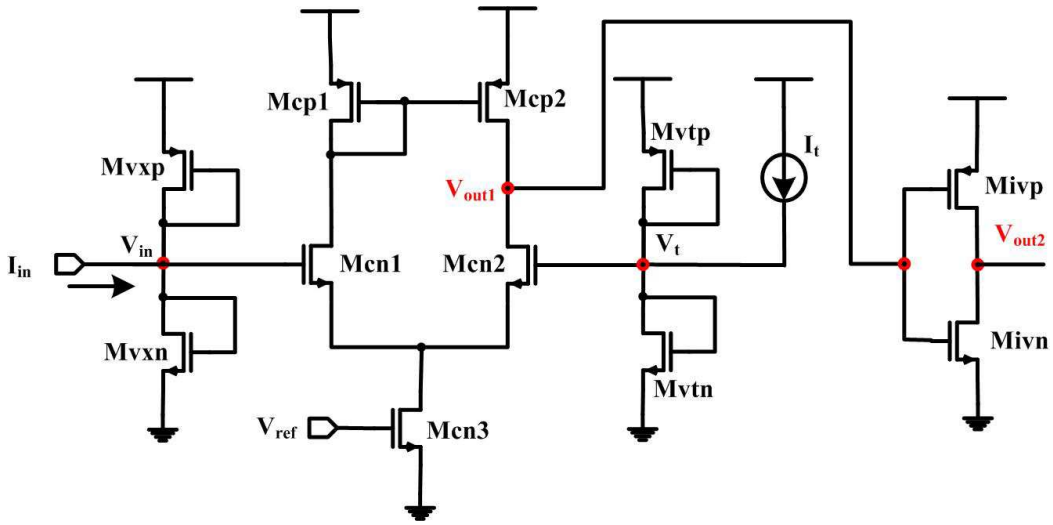

圖二：電流模式比較器

我們可以獲得當 $I_{in} > I_t$，可得 V_{out1} 為邏輯 1，V_{out2} 為邏輯 0，否則 V_{out1} 為邏輯 0，V_{out2} 為邏輯 1。其中 V_{out1} 及 V_{out2} 為互補的輸出。因此，我們可以將以此電流模式比較器作為控制分段電路的基礎。

其次，我們要介紹另一控制分段電路如圖三所示。

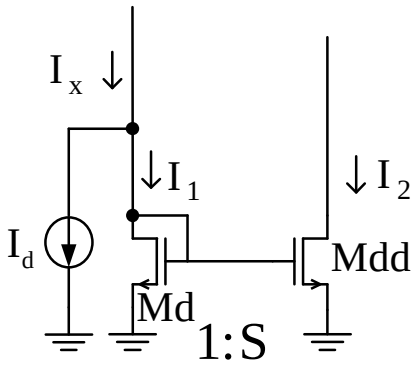

圖三：電流模式比較器

當 $I_x > I_d$，Md 導通，$I_2 > 0$，最後 $I_2 = SI_1$。

2、二次多項式電路

電路原理分析如下。由於 MOS 工作在飽和區時會有平方的特性，因此在設計上可使用[6]如圖四所示之電路架構，來實現電流模式的平方原理。假設圖四中 M1、M2 皆工作在飽和區且 K 值完全匹配，即 $K=K_n=K_p$，$K_p = \frac{1}{2}\mu_p C_{ox}\frac{W}{L}$，$K_n = \frac{1}{2}\mu_n C_{ox}\frac{W}{L}$，當輸入電流 I_x 之流向為流出時，I_x 會切分 I_1 與 I_2 兩電流，I_1 與 I_2 可分別表示為：

$$I_1 = K(V_{GS} - |V_{tp}|)^2 = K(V_{DD} - V_C - |V_{tp}|)^2 \tag{19}$$

$$I_2 = K(V_{GS} - |V_{tn}|)^2 = K(V_C - |V_{tn}|)^2 \tag{20}$$

$I_2=I_1-I_X$，將(19)與(20)代入得：

$$K(V_C - V_{tn})^2 = K(V_{DD} - V_C - |V_{tp}|)^2 - I_X \tag{21}$$

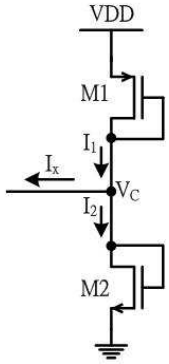

圖四：核心電路(平方電路)

整理(21)，以 I_X 為表示式：

$$I_X = K[V_{DD} - (V_C + |V_{tp}|)]^2 - K(V_C - V_{tn})^2$$

$$= K[V_{DD}^2 - 2V_{DD}(V_C + |V_{tp}|) + (V_C + |V_{tp}|)^2] - K(V_C^2 - 2V_C V_{tn} + V_{tn}^2)$$

$$= K(V_{DD}^2 + V_{tp}^2 - 2V_{DD}V_C - 2V_{DD}|V_{tp}| + 2V_C|V_{tp}| + 2V_C V_{tn} - V_{tn}^2)$$

$$= K[(V_{DD} - |V_{tp}|)^2 - V_{tn}^2] - 2K(V_{DD} - |V_{tp}| - V_{tn})V_C \quad (22)$$

在(22)式中，V_C 可表示成：

$$V_C = \frac{(V_{DD} - |V_{tp}| - V_{tn})(V_{DD} - |V_{tp}| + V_{tn})}{2(V_{DD} - |V_{tp}| - V_{tn})} + \frac{I_X}{2K(V_{DD} - |V_{tp}| - V_{tn})}$$

$$= \frac{(V_{DD} - |V_{tp}| + V_{tn})}{2} + \frac{I_X}{2K(V_{DD} - |V_{tp}| - V_{tn})} \quad (23)$$

將(23)代入(19)與(20)式，I_1 及 I_2 可表示成：

$$I_1 = K[\frac{V_{DD} - |V_{Tp}| - V_{Tn}}{2} + \frac{I_X}{2K(V_{DD} - |V_{Tp}| - V_{Tn})}]^2 \quad (24)$$

$$I_2 = K[\frac{V_{DD} - |V_{Tp}| - V_{Tn}}{2} - \frac{I_X}{2K(V_{DD} - |V_{Tp}| - V_{Tn})}]^2 \quad (25)$$

在(24)式與(25)式中，我們假設 $V_0 = \frac{V_{DD} - |V_{Tp}| - V_{Tn}}{2}$ 即可將方程式改寫成：

$$I_1 = KV_0^2(1 + \frac{I_X}{4KV_0^2})^2 \quad (26)$$

$$I_2 = KV_0^2(1-\frac{I_X}{4KV_0^2})^2 \tag{27}$$

圖五為二次多項式電路雛型，其原理是使用圖四的平方電路搭配電流鏡電流比值的關係，使用電流方式來達成 $I_{out}=I_0(ax^2+bx+c)$形式的二次多項式。

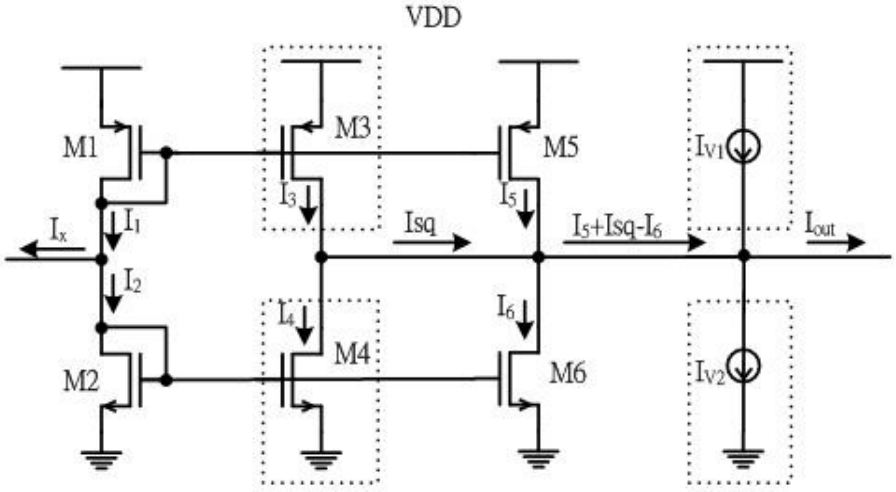

圖五：二次多項式電路雛型

在此二次多項式電路中 M1、M2 兩電晶體作用在於產生 I_1 與 I_2 兩電流作為主要 Miror 用電流，而 M3 與 M4 兩電晶體功能在於調整修正我們所想要的平方項 I_0 (ax^2)的部分，一次項 I_0bx 的部分由 M5 與 M6 來達成，而定電流 I_{V1} 與 I_{V2} 部分則是常數項 I_0c 部分的修正，利用此六顆 MOS 與定電流源可以達到我們所期望的二次多項式電路。

假設我們所有電晶體皆工作在飽和區且輸出電流為 $I_{out}=I_0(ax^2+bx+c)$，當輸入 I_x 電流時我們會從 M1、M2 兩電晶體得到 I_1 與 I_2 兩電流，其電流可分別表示為：

$$I_1 = KV_0^2(1+\frac{I_x}{4KV_0^2})^2$$

$$I_2 = KV_0^2(1-\frac{I_x}{4KV_0^2})^2$$

假設 $x=\frac{I_x}{mI_0}$ 可得 $I_x=mxI_0$ 我們可將 I_1、I_2 改寫成：

$$I_1 = KV_0^2(1+\frac{mI_0x}{4KV_0^2})^2 \tag{28}$$

$$I_2 = KV_0^2(1-\frac{mI_0x}{4KV_0^2})^2 \tag{29}$$

其中 m 值為一待定的常數，並且假設 $I_0 = KV_0^2$ 所以我們可從(28)、(29)式推得：

$$I_1 = I_0(1+\frac{mI_0x}{4I_0})^2 = I_0(1+\frac{mx}{4})^2 \tag{30}$$

$$I_2 = I_0(1-\frac{mI_0x}{4I_0})^2 = I_0(1-\frac{mx}{4})^2 \tag{31}$$

再將 I_3 從(30)式做 s 倍的電流鏡，I_4 也從(31)式做 s 倍的電流鏡，我們利用此兩電流對方程式中的平方項做調整，但值得注意的是當我們平方項係數 a 值是正值時，我們會選用 I_3 項電流做為調整用，若負值則用 I_4 項電流做為調整用，所以首先將 I_3 從(30)式做 s 倍的電流鏡，I_4 也從(31)式做 s 倍的電流鏡可得：

$$I_3 = sI_0(1+\frac{mx}{4})^2 \tag{32}$$

$$I_4 = sI_0(1-\frac{mx}{4})^2 \tag{33}$$

我們也可以利用 I_5 從(30)式做 r 倍的電流鏡，I_6 也從(31)式做 r 倍的電流鏡來對方程式中的一次項做調整，可得：

$$I_5 = rI_0(1+\frac{mx}{4})^2 \tag{34}$$

$$I_6 = rI_0(1-\frac{mx}{4})^2 \tag{35}$$

在常數項的 I_V 部分，我們是將電流乘上一個 q 值的倍率來做修正，若常數項(c)為正值，則使用電流源(I_{V1})，若常數項為負值得時候，則使用電流源(I_{V2})，並假設

$$I_{V1}=I_{V2}=qI_0 \tag{36}$$

假設多項式 ax^2+bx+c 中的係數 a、b、c 值皆為正值，從(32)、(34)、(35)、(36 及圖五可得：

$I_{out}=I_5+I_{sq}-I_6+I_{V1}$

$$= rI_0(1+\frac{mx}{4})^2 + sI_0(1+\frac{mx}{4})^2 - rI_0(1-\frac{mx}{4})^2 + qI_0$$

整理後可得：

$$= I_0[(\frac{sm^2}{16})x^2 + (\frac{sm}{2}+rm)x + (s+q)] \tag{37}$$

而 $$I_{out}=I_0(ax^2+bx+c) \tag{38}$$

比較(37)式與(38)式可得：

$$[ax^2+bx+c] = [(\frac{sm^2}{16})x^2 + (\frac{sm}{2}+rm)x + (s+q)]$$

$$a = \frac{sm^2}{16} \tag{39}$$

$$b = \frac{sm}{2} + rm \tag{40}$$

$$c = s + q \tag{41}$$

將(39)式、(40)式、(41)式，整理成 s、r、q 各電流鏡比值表示形式：

$$s = \frac{16a}{m^2} \tag{42}$$

$$r = \frac{b}{m} - \frac{|s|}{2} \tag{43}$$

$$q = c - s \tag{44}$$

我們可依據(42)(43)(44)三式來調整電晶體內 W/L 比，以求得電路中我們所需的 W/L 值。在此設計中，我們又能依據使用者所訂定的 a、b、c 係數，來對電路調整比值以達到使用者所需要的二次多項式組合。

3、整合電路：

圖五之二次多項式電路雛型為二次多項式電路之一般型，真正使用的電路，並非 M3、M4、M5、M6、I_{v1} 及 I_{v2} 都使用到，如圖六、七所示，圖六是當 ax^2+bx+c 中的係數 a、b、c 值皆為正值，所使用的電路；而圖七則是 a、b、c 值為"負正負"時，所使用的電路。

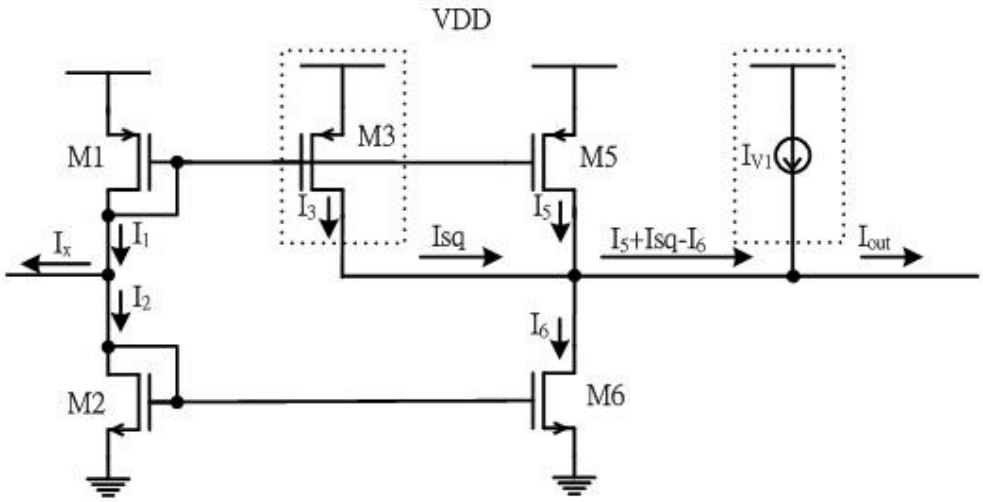

圖六：二次多項式電路(a,b,c 係數為正正正型式)

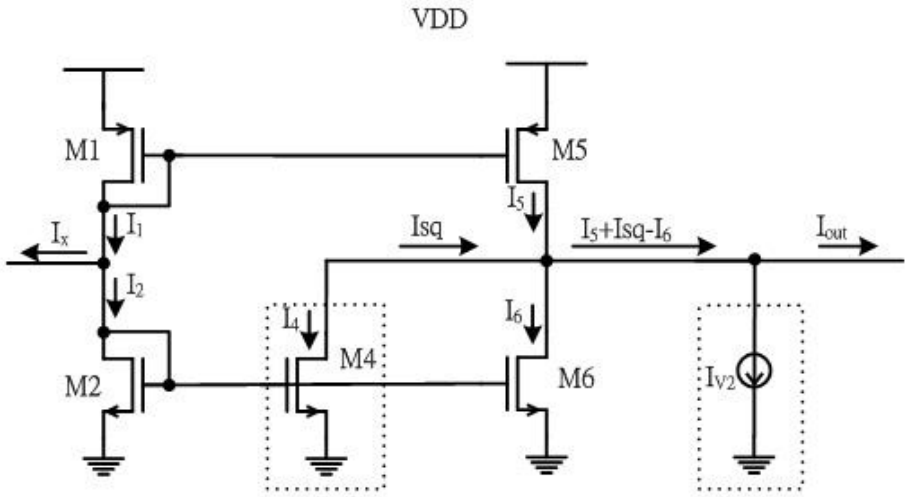

圖七：二次多項式電路(a,b,c 係數為負正負型式)

我們將圖五之二次多項式電路雛型加上控制界面如圖八，圖中 V_{out} 受前述之控制分段電路 V_{out} 控制。假設要實現一 f(x)函數，我們將輸入範圍分為兩段，分別使用 Taylor 的二次多項式展開為 $a_1x^2 + b_1x + c_1$ 及 $a_2x^2 + b_2x + c_2$。實現步驟以圖九來表示，圖中(A)方塊為圖二之電路；(B)(C)方塊為圖八之電路，電流 I_t 為分段處的電流。

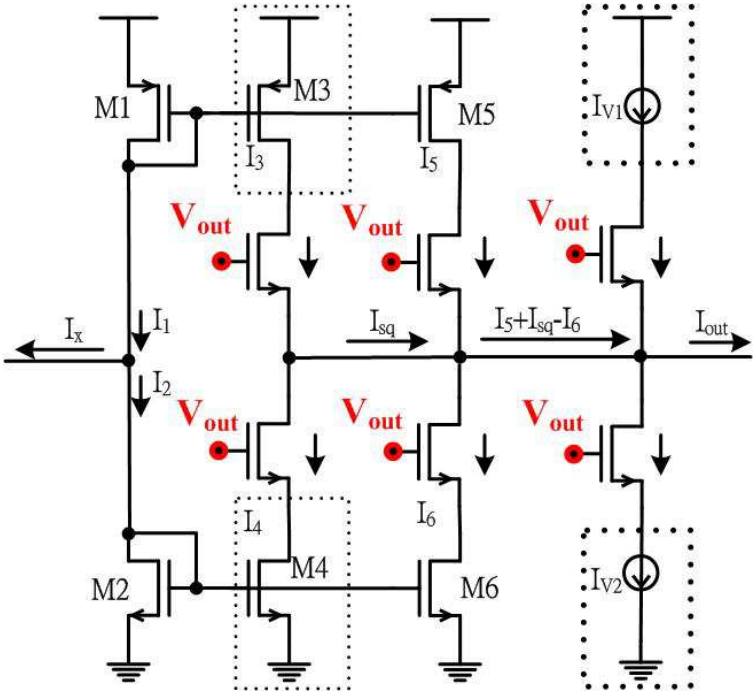

圖八：具有控制界面之二次多項式電路

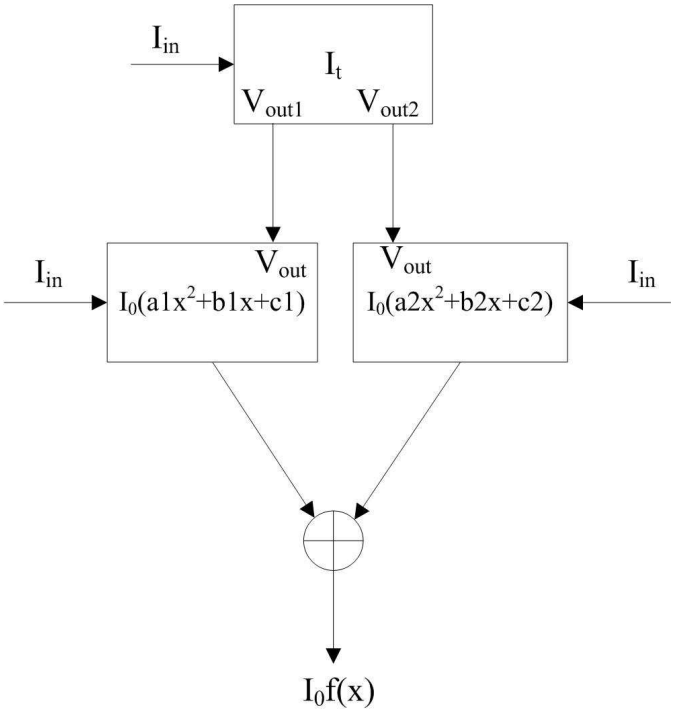

圖九：二分段之函數產生方塊圖

4、模擬電路結果：

Sigmoid 函數在神經網路中被廣泛使用，如 Artificial neural networks(ANN)與 Fuzzy networks(FNN)。在人工神經網路(ANN)的硬體實現上，非線性函數的計算對於影響系統使用的面積或延遲時間為重要因素。本模擬電路是利用多段方式實現 Sigmoid 函數電路為例來提升 Sigmoid 函數之準確度、速度與寬輸入電流為目的，應用 CMOS 電流模式之方法，並創新以類比電路方式做分段的概念將 Sigmoid 函數實現。以往用 Gradient-descendent type 演算法計算 Sigmoid 函數過於複雜，這裡以較簡單的泰勒二階展開式取代，由於泰勒二階展開式相對較不準確近而搭配分段的概念，將 Sigmoid 函數分成四段實現，而完成高準確度、速度快與寬輸入電流之 CMOS 電流模式 Sigmoid 函數電路。

Sigmoid 電路架構由四個主要方塊組成如下(圖十)，分別為 current source、second-order circuit、current control switch、multi segment。current source 設計目的為提供多個 second-order circuit 輸入電流，second-order circuit 為實現各分段之電路，current control switch 是作為控制個分段電路導通之用，multi segment 合成個分段電路。Multi-segment 架構目的在於利用簡單二次多項式電路實現複雜不同的函數，提高準確度並節省面積。

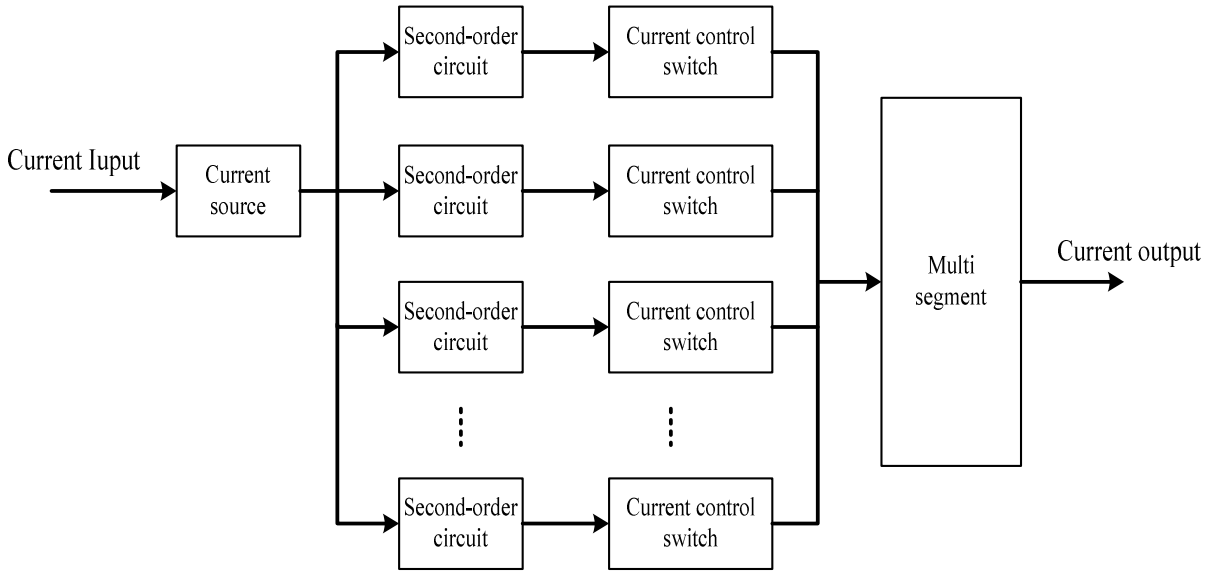

圖十：Sigmoid 電路架構之四個主要方塊圖

current source(圖十一)由多組電流鏡組成，在單一輸入電流下轉換提供下級所許之多個輸入電流。

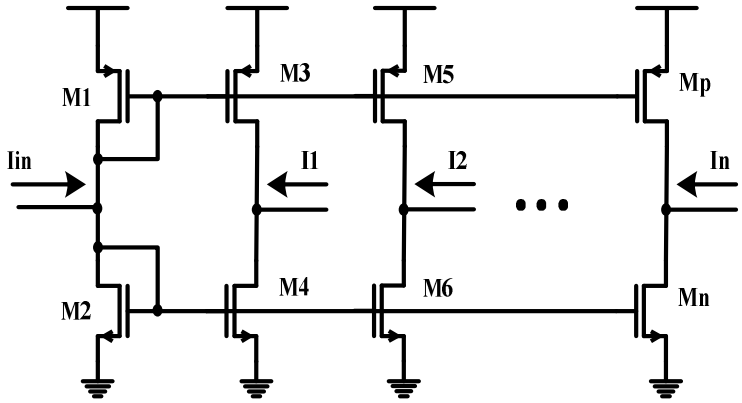

圖十一：多組電流鏡電路圖

second-order circuit(圖十二)由簡易二次多項式電路將實現之函數分成多段製作，利用分段電路提升整體函數之準確度。

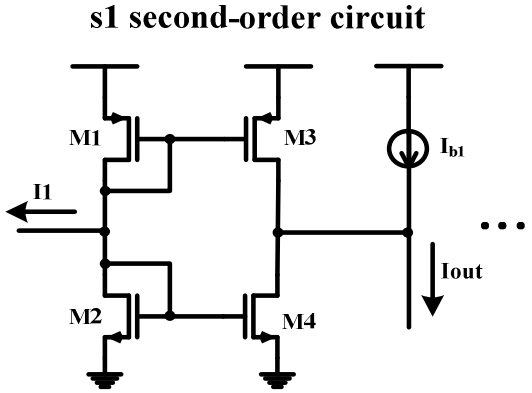

圖十二：二次多項式電路圖

current control switch(圖十三)在一個較大輸入電流下，以定電流源控制所需分段之電流端點進行切割，並以 inverter 特性做 I-V 轉利用換搭配不同電壓做切換控制。

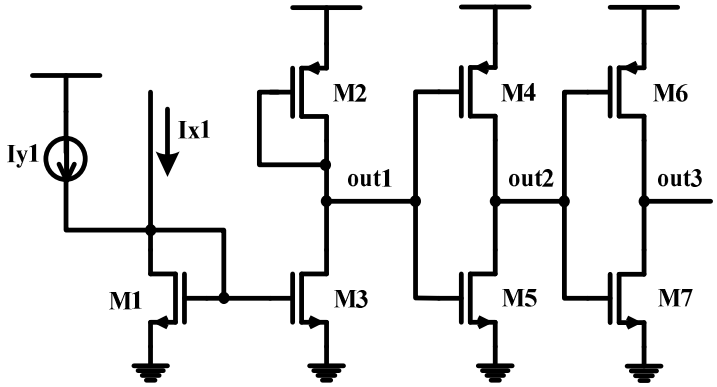

圖十三：定電流源控制分段電路圖

multi segment(圖十四)將電流控制電路轉換出分段電壓，經由 NMOS 做整體電路合成，最後實現所需之函數。

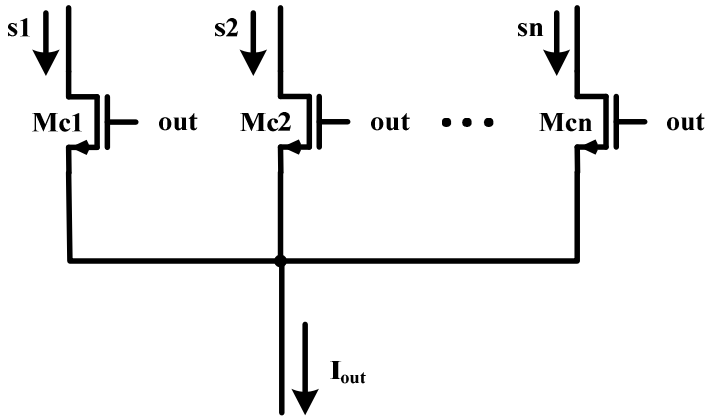

圖十四：NMOS 電路合成圖

圖十五為實現 Sigmoid 函數之整體電路圖。

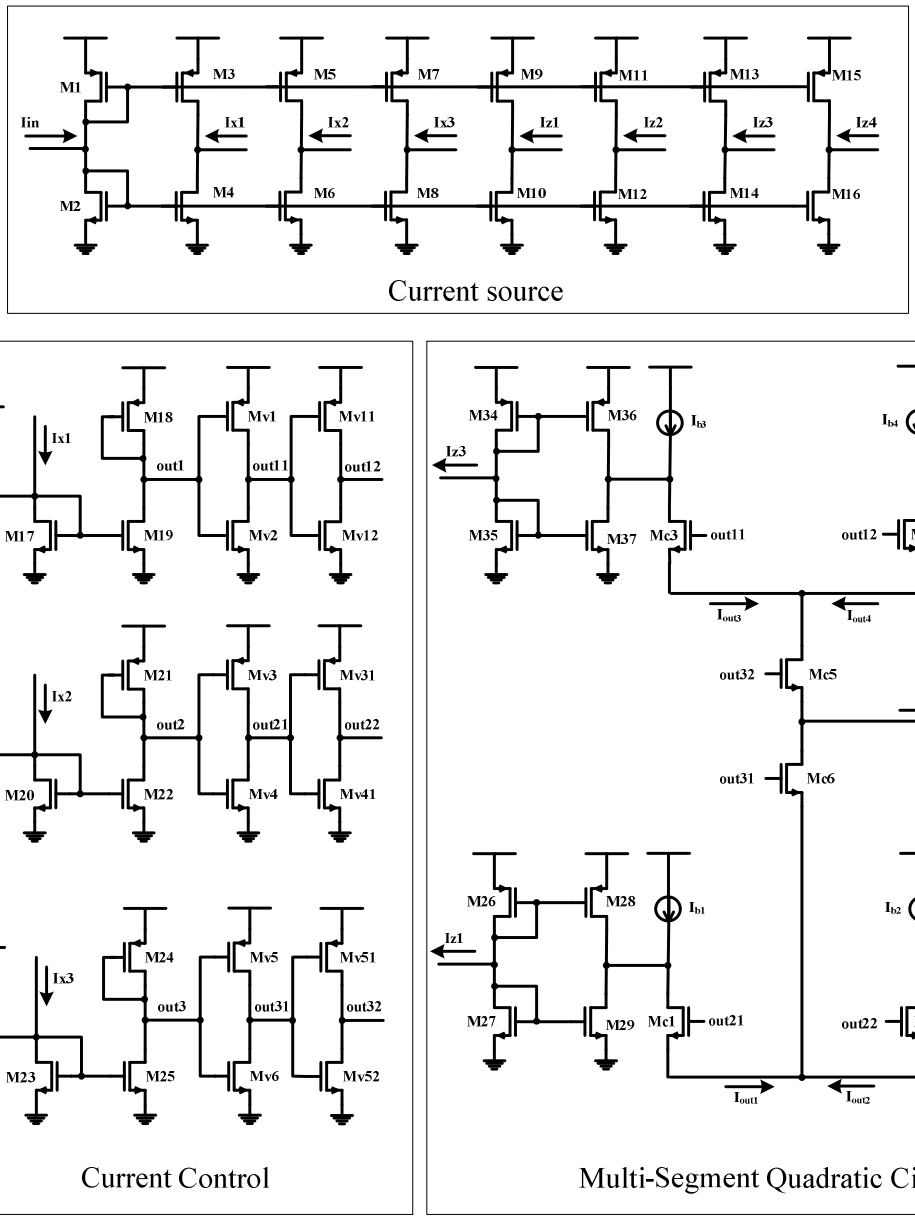

圖十五：Sigmoid 函數電路圖

5、晶片製作：

晶片製作規格列表如下：

電路名稱：利用多段趨近法設計高準確度 CMOS 電流模式 Sigmoid 電路

Technology：TSMC 0.18 um CMOS Mixed Signal RF General Purpose Standard Process FSG Al 1P6M 1.8&3.3V

Package：18 S/B DIP

Transistors/MOS Count：82 MOS

Chip Size : 0.32×0.32 um^2

Power Dissipation：4.27 mW

此電路模擬之輸入電流 I_{in}=-400μA~400μA，V_{DD}=1.8V。圖十六為 pre-simulation 與 post-simulation 輸出電流比較圖與絕對誤差圖，對於電路變異上，應用蒙地卡羅分析，亂數模擬 30 次中，百分之八十相對誤差都在 3%以內。

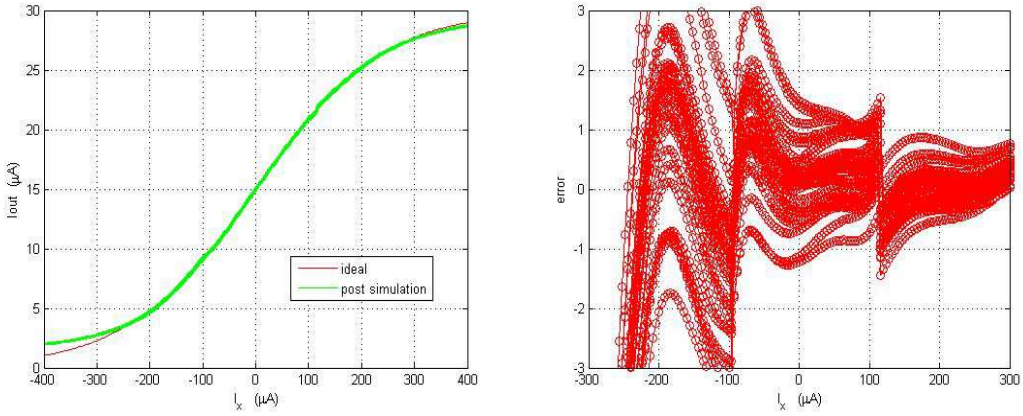

圖十六： pre-simulation 與 post-simulation 及蒙地卡羅分析圖

圖十七為 TT、FF、FS、SF、SS 各種不同狀態下的模擬圖。

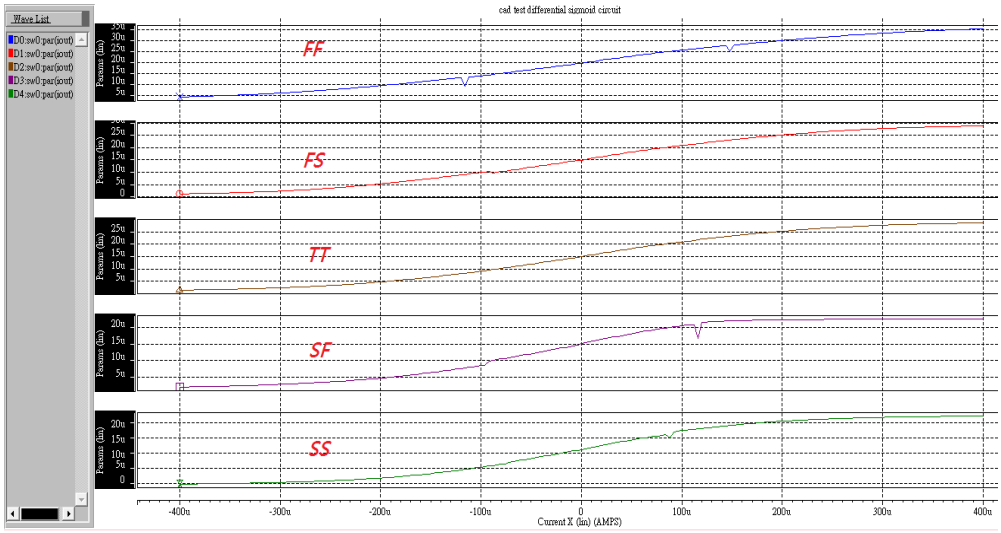

圖十七：TT、FF、FS、SF、SS 模擬圖

電壓變動對此電路影響，應用 PSRR 做為模擬(圖十八)，此電路 PSRR 為 71.4。

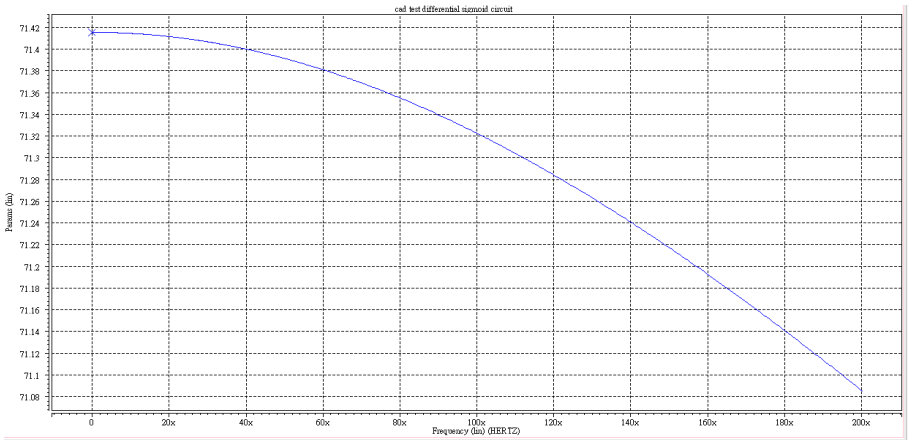

圖十八：PSRR 模擬圖

圖十九為 pre-simulation 與 post-simulation 電路頻寬模擬圖。

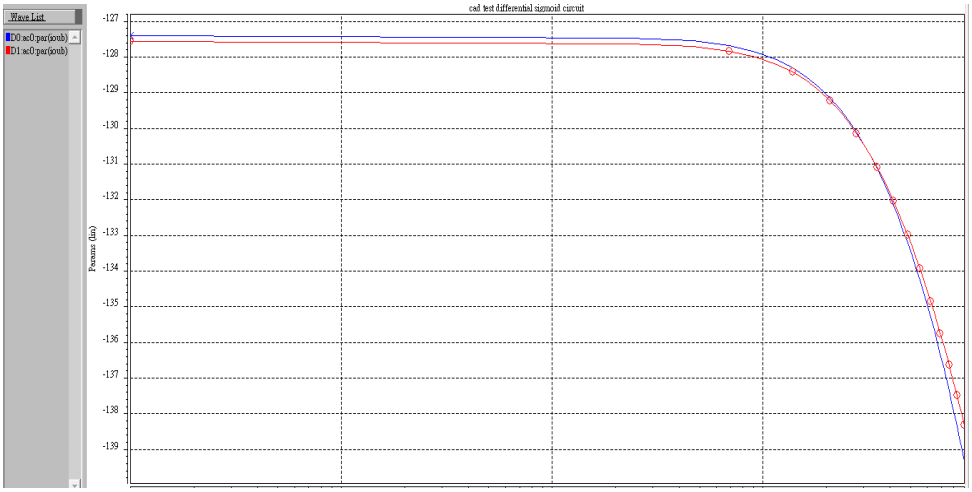

圖十九：電路頻寬模擬圖

打線圖如下：

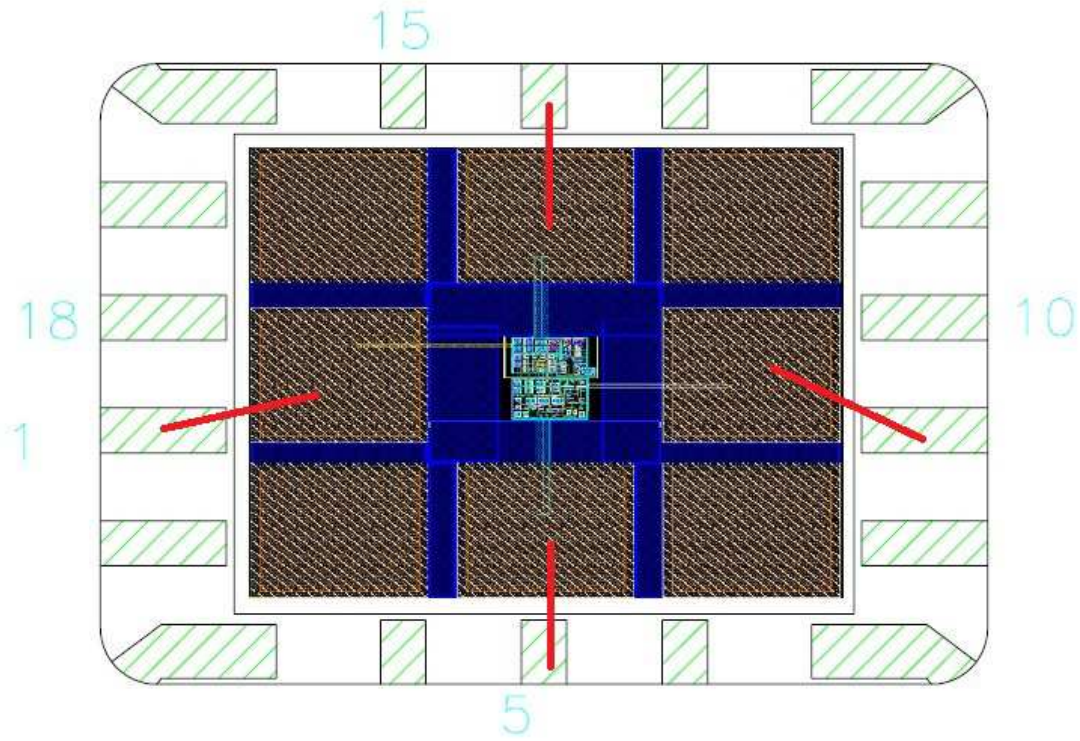

測試規格如下列表：

Parameter	Spec.	Pre-simulation	Post- simulation
Power Supply(V)	1.8	1.8	1.8
Input range(μA)	±400	±400	±400
Input Voltage(V)	0.38 ~ 0.9	0.38 ~ 0.9	0.38 ~ 0.9
Output Voltage(V)	<0.85	0.7 ~ 0.83	0.7 ~ 0.83
Power Dissipation(mW)	<4.3	4.272	4.284
Oscillator Frequency(MHz)	<308	308	297
Chip size (mm^2)	0.33x0.33	0.32 x 0.32	

文獻比較表如下：

	This work	Abu.,M.T. 2006[25]	Chun Lu 2002 [26]	Genov, R. 2004[27]
Tech. CMOS	0.18μm	0.18μm	0.5μm	0.5μm
Vdd(V)	1.8	1.8	3.3	1.5
Power Consumption(mW)	4.283	x	10	82
Input range(μA)	±400	-25~0	x	x
Input range(V)	0.38 ~ 0.9	x	x	1.8~3.2
Bandwidth(MHz)	308	x	x	128
Chip size (mm^2)	0.32x0.32	x	1.5 x 0.7	0.7 x 2

本電路應用 TSMC 0.18μm 製程，Power 消耗相較於[26-27]低。在 Input range 以 CMOS 電流模式範圍擴展之多段法，使輸入電流為±400μA 遠大於[25]文獻。頻寬上更可達到 308MHz，大於[27]文獻。Chip size 為 0.32 x 0.32 小於[26-27]文獻。

在測試晶片的階段，由於電源供應器無法提供輸入電流±400μA，因而利用輸入輸出兩個節點做 I-V 轉換，其電流範圍的電壓值在 0.38 V~ 0.9V 間，我們量測上主要使用電壓方式去量測結果。所使用設備有電源供應器與數位式示波器，其中電源供應器提供.38 V~ 0.9 V 的輸入電壓，而數位式示波器用來量測輸出值，若輸出端電壓量測結果為 0.7 V~ 0.83V，即可推出輸出電流是否正確。

五、結果與討論

本研究計畫之 CMOS 電流模式多分段控制二次多項式電路已發展完成，在 ICEOE 2012 國際會議中發表兩篇 EI 論文[28][29]。在[28]中，利用電流比較器的方式做分段控制。在[29]中，則是利用差動放大器的方式做分段控制。另外，二次多項式電路的應用也被 IEICE 期刊接受，預計於 2012 的 11 月刊登[30] 。本研究計畫之實作晶片預計於 2012 的 11 月產出。我們可以從 Post-Simulation 中看出當溫度及 VDD 固定在要求的範圍時，可以保證在 3%的相對誤差範圍內，達到高輸入動態範圍的要求，輸入電流從-400 μA 到 400 μA，克服了一般非分段的方法之範圍限制。

六、參考文獻

[1] Kuo-Jen Lin, “Two-Quadrant CMOS Plug-in Divider,” IEICE Trans. Fundamentals., Vol.E91-A, No. 9, pp. 2682-2684, 2008.

[2] Kuo-Jen Lin, “CMOS Current-Mode Companding Divider,” IEICE Trans. Electron., Vol.E92-C, No. 3, pp. 380-382, 2009.

[3] Kuo-Jen Lin, “Two-Quadrant Compact CMOS Current Divider,” IEICE Trans. Fundamentals., Vol.E92-A, No. 7, pp.1713-1715, 2009.

[4] Kuo-Jen Lin and Chih-Jen Cheng, “CMOS Nth-Switchable-Root Circuit,” IEICE Trans. Electron., Vol.E93-C, No. 1, pp. 145-147, 2010.

[5] Kuo-Jen Lin and Chih-Jen Cheng, “CMOS Current-Mode Geometric-Mean Circuit with N Inputs,” IEEE International Symposium on Signal, Circuits & Systems, Iasi, Romania, pp. 1-4, Jul. 9-10, 2009.

[6] A. Ravindran, K. Ramarao, E. Vidal, and M. Ismail, “Compact low voltage four quadrant CMOS current multiplier," Electron. Lett., vol.37, no.24, pp.1428-1429, 2001.

[7] C. Toumazou, F.J. Lidgey, and D.G. Haigh, Analogue IC Design: the current mode approach, Peter Peregrinus, London, 1990.

[8] B. Wilson, “Recent developments in current conveyors and current-mode circuits,” IEE Proc. G, 137, pp. 63-77, 1990.

[9] A.F. Arbel and L. Goldminz, “Output stage of current-mode feedback amplifiers, theory and applications,” Analog Integrated Circuits and Signal Processing, 2, pp.243-255, 1992.

[10] A.F. Arbel, J.E. Bowers, and J. Lauch, “Low-noise high-speed optical receiver for fiber optic systems,” IEEE J. Solid-State Circuits, 19, pp. 155-157, 1984.

[11] T. Kaulberg, “A CMOS current-mode operational amplifier,” IEEE J. Solid-State Circuits, 28, pp. 849-852, 1993.

[12] H. Song, C. Kim, “A MOS four-quadrant analog multiplier using simple two-input squaring circuits with source followers,” IEEE J. Solid-State Circuits, SC-25, pp. 841-894, 1990.

[13] Z. Wang, “A MOS four-quadrant analog multiplier with single-ended voltage output and improved temperature performance,” IEEE J. Solid-State Circuits, SC-26, pp. 1293-1301, 1991.

[14] T.S. Lande, J.A. Nesheim, Y. Berg, “Auto correlation in micropower analog CMOS,” Analog Integr. Circuits Signal Process, 1, 1995, pp. 61-68, 1995.

[15] R.J. Wiegerink, “Analysis and synthesis of MOS translinear circuits,” Kluwer, Boston, 1993.

[16] C.Y. Huang, C.Y. Chen, B.D. Liu, “Current-Mode Fuzzy Linguistic Hedge Circuits,” Analog Integr. Circuits Signal Process, 19(3), pp. 255-278, 1999.

[17] C.A. De La Cruz-Blas, A. Lopez-Martin, A. Carlosena, “1.5-V MOS Translinear Loops with Improved Dynamic Range and Their Applications to Current-Mode Signal Processing,” IEEE Trans. Circuit Syst.-II, 50(12), pp. 918-927, 2003.

[18] J.K. Seon, “Design and application of precise analog computational circuits,” Analog Integr. Circuits Signal Process, 54, pp. 55-66, 2008.

[19] S. Menekay, R.C. Tarcan, H. Kuntman, “Noval high-precision current-mode circuits based on the MOS-translinear principle,” AEU Int. J. Electron. Commun., 63, pp. 992-997, 2009.

[20] T. Rungkhum, A. Julsereewong, V. Riewruja, P. Julsereewong, “A CMOS-based Square-Rooting Circuit,” International Conference on Control, Automation and Systems, pp. 161-164, 2007.

[21] W. Petchakit, A. Lorsawatsiri, W. Kiranon, C. Wongtaychathum, P. Wardkein, “Current-mode squaring, square-rooting and vector summation circuits,” AEU Int. J. Electron. Commun., 64, pp. 443-449, 2010.

[22] M. mottaghi-kashtiban, A. Khoei, K. Hadidi, “A Current-Mode, First-Order Takagi-Sugeno-Kang Fuzzy Logic Controller, Supporting Rational-Powered Membership Functions,” IEICE TRANS. Electron., E90-C(6), pp. 1258-1266 2007.

[23] A. Motamed, C. Hwang, M. Ismail, “CMOS exponential current-to-voltage converter,” Electron. Lett., 33(12), pp. 998-1000, 1997.

[24] N. Onizawa and T. Hanyu, “Robust multiple-valued current-mode circuit components based on adaptive reference-voltage control,” 39th International Symposium on Multiple-Valued Logic, pp. 36-41, 2009.

[25] M. T. Abuelma'ati and A. Shwehneh, “A Reconfigurable Satlin/Sigmoid/Gauusian/Triangular Basis Functions Computation Circuit,” IEEE International Conference on Computer Systems and Applications,pp. 232 – 239, 2006.

[26] Chun Lu, Bingxue Shi, and Lu Chen, “A general-purpose neural network with on-chip BP learning,” IEEE International Symposium on Circuits and Systems, pp. 520-523, 2002.

[27] R. Genov and G. Cauwenberghs, “Dynamic mos sigmoid array folding analog-to-digital conversion,” IEEE Transactions on Circuits and Systems I Regular Papers, pp. 182-186, 2004.

[28] Kuo-Jen Lin, Chih-Jen Cheng, and Jwu-E Chen, “Multi-Point Correction Method in CMOS Current-Mode Function Design,” 2nd International Conference on Electronics and Optoelectronics, Shenyang, China, pp. 294-298, 2012.

[29] Chih-Jen Cheng, Kuo-Jen Lin, and Jwu-E Chen, “CMOS Current-Mode Hyperbolic Tangent Sigmoid Function Implementation Using Multi-Segment Approximations,” 2nd International

Conference on Electronics and Optoelectronics, Shenyang, China, pp. 299-303, 2012.

[30] Kuo-Jen Lin, Chih-Jen Cheng, Hsin-Cheng Su, and Jwu-E Chen “A CMOS Current-Mode S-Shape Correction Circuit with Shape-Adjustable Control,” IEICE Trans. Electron., Vol.E95-C, No. 11, pp. --, 2012.

七、計畫成果自評

國科會補助專題研究計畫成果報告自評表

請就研究內容與原計畫相符程度、達成預期目標情況、研究成果之學術或應用價值（簡要敘述成果所代表之意義、價值、影響或進一步發展之可能性）、是否適合在學術期刊發表或申請專利、主要發現或其他有關價值等，作一綜合評估。

1. 請就研究內容與原計畫相符程度、達成預期目標情況作一綜合評估 ■ 達成目標 □ 未達成目標（請說明，以 100 字為限） □ 實驗失敗 □ 因故實驗中斷 □ 其他原因 說明：
2. 研究成果在學術期刊發表或申請專利等情形： 論文：■已發表 □未發表之文稿 □撰寫中 □無 專利：□已獲得 □申請中 ■無 技轉：□已技轉 □洽談中 ■無 其他：（以 100 字為限）

3. 請依學術成就、技術創新、社會影響等方面，評估研究成果之學術或應用價值（簡要敘述成果所代表之意義、價值、影響或進一步發展之可能性）（以500 字為限）

本研究計畫利用分段趨近的方式，提出實現的電路與趨近的二次多項式電路來達成所要表達的複雜函數電路。所使用的電路特色是電流模式，能更擴大所需要的動態輸入範圍，可貢獻在可變增益放大器的應用上及一些複雜函數的實現，例如應用 Sigmoid 的類神經網路等學術應用。

在分段的技術上，我們採用電流控制的方式來切割段落。然而每個段落的二次多項式電路也必須精準地表現該段落的曲線，因此在控制分段的電路與二次多項式電路及輸入電流大小之間的介面就容易造成偏差，因此我們使用特別設計的定電流模組，將造成偏差的因素，由定電流模組來共同解決。

因為有大的動態輸入範圍，如果應用於手機通訊上的可變增益放大器放大來自基地台的微弱訊號，將可大幅提高手機的收訊品質。另外如果應用於類神經網路，則可將手機帶入更智慧型的領域。當然，更進一步的發展，必須搭配更深入的研究，例如針對特定的精度要求，我們必須分割更多段數來完成，而多少的段數及多大的範圍是電路所不能負擔的，皆需要進一步的研究。對於可變增益放大器的實作上，也要下點功夫，研究適當的演算法來實現較低功率的電路。

八、可供推廣之研發成果資料表

無。

九、附錄

本研究計畫論文發表共計兩篇國際會議論文及一篇 SCI 期刊論文如下:

1. Kuo-Jen Lin, Chih-Jen Cheng, and Jwu-E Chen, “Multi-Point Correction Method in CMOS Current-Mode Function Design,” 2nd International Conference on Electronics and Optoelectronics, Shenyang, China, 2012. (EI)

2. Chih-Jen Cheng, Kuo-Jen Lin, and Jwu-E Chen, “CMOS Current-Mode Hyperbolic Tangent Sigmoid Function Implementation Using Multi-Segment Approximations,” 2nd International Conference on Electronics and Optoelectronics, Shenyang, China, 2012. (EI)

3. Kuo-Jen Lin, Chih-Jen Cheng, Hsin-Cheng Su, and Jwu-E Chen “A CMOS Current-Mode S-Shape Correction Circuit with Shape-Adjustable Control,” IEICE Trans. Electron., Vol.E95-C, No. 11, pp. --, 2012. (SCI)

ICEOE2012 and OEMR2012 CONFERENCES SCHEDULE

2012 2nd International Conference on Electronics and Optoelectronics (ICEOE 2012)

2012 International Meeting on Opto-Electronics Engineering and Materials Research (OEMR 2012)

Tianlun Regar Hotel Shenyang

Shenyang, China

July 27 - 28, 2012

July 27, 2012 (Friday)

Lobby of Tianlun Regar Hotel Shenyang (沈阳天伦瑞格酒店大厅)

10：00 – 12：00 14：30 – 18：00	Arrival and Registration

Note：(1) You can also register at any time during the conference.

(2) Certificate of Participation can be collected at the registration counter.

(3) The organizer won't provide accommodation, and we suggest you make an early reservation.

Morning, July 28, 2012 (Saturday)

RUIHE A Hall of The Sixth Floor

6 层瑞和 A 厅

Time: 9:00-12:00

OE0150	Characteristic of Point Defect around the Photonic Crystal Bend
	Ruei-Chang Lu, Chun-Min Wang and Keh-Yi Lee
OE0151	Wavelength Division Multiplexer based on Periodic Dielectric Waveguide Ring Resonator
	Ruei-Chang Lu, Tung-Hao Chen and Yu-Ping Lia
OE0800	A new design of large area MCP-PMT for the next generation neutrino experiments
	Sen. Qian
OE0183	Noise Analysis of EMCCD and Optimum Design of Its Operating Mode
	Yugui Zhang,Tao Li and Zhikuan He
OE0590	Optimal Design of CCD Driving Signal Based on FLEX 10K
	Zhikuan He, Songbo Wu and Yugui Zhang
OE0239	A 5-port Photonic Lantern for Light Beam Combining
	Yan Qi, Haijiao Yu,Fengjun Tian and Weimin Sun
OE0539	CPU Experiment of Heat Dissipation and Temperature Rise
	Maode Li,Wei Wei and Yi Li
OE0235	Influence of Pump Light's Duty Cycle on Cesium Atomic Magnetometer
	Xianjin Zeng, Junhai Zhang, Qiang Liu, Zongjun Huang and Weimin Sun
OE0645	Influence of Plasmonic Light-Scattering by Gold Nano-island Structures on the Quantum Efficiency of Organic Solar Cell
	Baozeng Wang,Xinping Zhang and Jian Zhang
OE0646	Directly-Written Metallic Photonic Crystals for Sensor Applications
	Jian Zhang,Xinping Zhang,Zhaoguang Pang and Baozeng Wang
OE0195	The Effects of Pump Beam on Cesium Magnetometer Sensitivity
	Qingmeng Li, Qiang Liu, Junhai Zhang, Zongjun Huang, Xianjin Zeng and Weimin Sun
OE0584	Measurement of SO2 using Differential Optical Absorption Spectroscopy
	Haiming Zheng, Zhenliang Dong, Dongshui Xie and Xiaoxiao Shang

OE0109	Study On Control Technology of Double-fed Motor Based On PLC and General Invert
	Chengwu Lin, Jialin Shi and Bo Lu
OE0110	Research on Grid-connected Inverter Based on Current Track Control in Wind Generation System
	Chengwu Lin, Qiguang Jiang and Li Ma
OE0568	A new Coupled PDE Method for Image Processing
	Maolin Wang, Jun Yue, Pan Huang and Chaoshuai Song
OE0214	Comparison of Gold and Silver Nanoparticles as Active Substrates for SERS Spectra Measurements on Liver Cancer Cells
	Chen Qian,Shupeng Liu,Na Chen,Zhenyi Chen and Qianqian Geng
OE0202	Generation of Multi-Atom W States in Microtoroidal Cavity-Atom System
	Yu Huang
OE0165	A Method for Lidar Data Conversion and Standardization
	Hao Chen, Dengxin Hua, Yikun Zhang, Zhirong Zhou, Shichun Li and Li Wang
OE0233	The structural design of combined absorber composed by MPP and multi-layer porous material based on VA One
	Xiuhua Duan, Huanqin Wang,Wenjuan Sun and Deyi Kong
OE0537	Studying Relative Error Formulae of Surveying Textbooks of Chinese Colleges
	Yonghe Deng
OE0245	Dynamically manipulating beam with metallic nano-optic lens containing liquid crystal
	Jicheng Wang, Xia Zhou,Jie Gao,Zhetao Xu, Lin Sun and Xiao Jin
OE0550	Solvothermal method preparation of nano Y2O2SEu3+ and research of luminescence property
	Lu Lu and Zhilong Wang

12：00 - 13：30	Lunch Break

Afternoon, July 28, 2012 (Saturday)

RUIHE A Hall of The Sixth Floor

6 层瑞和 A 厅

Time: 14:00-18:00

CE0105	Fault diagnosis of COIL based on BP Artificial Neural Network
	Zheng Zhang, Shiqiang Zhang, Yanhong Sun
CE0121	Study of Top Triangular Nano-grating on Solar Cell Using Rigorous Coupled Wave Analysisg
	Xiaomin Jin, Douglas Alan Cattarusa, and Michael James Marshall
CE0126	Comparative Research on Different Solutions of a High-Performance Thin-Film Polarizing Beam Splitter
	Kaiyong Yang, Hongchang Zhao, Yunfeng Jia, Suyong Wu
CE0140	Optimization Of Fiber Length For Edfa To Enhance The Channel Capacity Of Dwdm System
	Inderpreet Kaur, Neena Gupta
CE0143	Long-haul Wavelength Division Multiplexing Secure Communications with Chaotic Optical Channels
	Xiaolei Chen, Qingchun Zhao, Hongxi Yin, Xinyu Dou
CE0145	Optical-Mode Study of Galium Nitrate Based Laser Diodes
	Douglas Alan Cattarusa, Xiaomin Jin, Xiao-Hua Yu, Xing-Xing Fu, Xiang-Ning Kang, Bei Zhang, Guo-Yi Zhang
CE0157	A simple mechanism to suppress the mode competition for stable and tunable dual-wavelength erbium-doped fiber lasers
	Chenfang Zhang, Jiang Sun, Siwen Zheng and Shuisheng Jian
CE0166	Application of Optical Phase conjugation in Adaptive optics to remove atmospheric aberrations from an optical wavefront
	Sriram Rengarajan, Nandhakishore Perarulalan
CE0172	Study on Optical Performance Monitoring for Fiber-optical Link Utilizing Chaos Theory
	Qingqing Fan, He Li, Hongxi Yin
CE0186	Multi-Point Correction Method in CMOS Current-Mode Function Design
	Kuo-Jen Lin, Chih-Jen Cheng, Jwu-E Chen
CE0199	CMOS Current-Mode Hyperbolic Tangent Sigmoid Function Implementation Using Multi-Segment Approximations
	Chih-Jen Cheng, Kuo-Jen Lin, Jwu-E Chen
CE0235	The development of Remote Measurement System Based on GSM Internet of Things(IOT)
	Yunxin Gong, Houyu Zhao
CE0245	Research of Temperature Compensation for Ultrasonic Rangefinder
	Gang Tian, Jun Gui
CE0247	Analysis on the Relationship Between Burst Errors and Tracking Control Frequency in Satellite-to-Ground Laser communications
	Qiwen Ran, Zhonghua Yang, Jing Ma, Liying Tan, Shichen Wu, Qingfeng liu, Huixi

	Liao
CE0273	The three-dimensional analysis of light scattering characters for Rayleigh particles on/below the wafer
	Lei Gong, Zhensen Wu
CE0282	Simulation of Laser Beam Scattering from Complex Targets in the Near Field
	Jiaxuan Lin, Zhensen Wu, Xiang Su, Biao Wang
CE0284	The Analysis of Influencing Factors of One Dimensional Range Profiles and Surface Elements Imaging Method to Arbitrary Target
	Yuan Mou, Zhensen Wu, Zhuo Chen, Hanlu Zhang
CE0285	Scattering Properties of the Higher-Order Hermite Gaussian Beam
	Tan Qu, Zhensen Wu, Haiying Li, Zhengjun Li
CE0287	Extraordinary Electromagnetic Scattering of Plane Wave by Double Negative Coated Sphere
	Yan'e Shi, Zhensen Wu, Hongfei Tian, Zhengjun Li
CE0288	Scattering Characteristics of Complex Target from Solar Irradiance and Sky-ground Background Radiance in Infrared Spectrum
	Xing Guo, Zhensen Wu, Longxiang Linghu, Yufeng Yang
CE0289	Scattering of Two-Dimensional Sea Surface at Low Grazing Angles with Physical Optics Method
	Zhuo Chen, Zhensen Wu, Yong Zhang, Jingjing Xue, Wenhua Ye
CE0292	The Acceleration of PO Based on CUDA
	Xiang Su, Zhensen Wu, Jiaxuan Lin and Xiaobing Wang
CE0293	Decomposing the Non-Gaussian Surface in Sum of Gaussian Surfaces
	Zhangxing Qi, Zhensen Wu, Ziwen Yu, Haiying Li
CE0294	Polarization Properties of Scattered Fields from a Chiral Sphere
	Qingchao Shang, Zhensen Wu, Peng Zhao, Zhengjun Li
CE0311	Phase-only Beam Optimization for GaAs Optical Waveguide Phase Array
	Yong Zhang
CE0314	Path loss of Non-Line-of-Sight single-scatter model
	Tairong Wang, Lu Bai, Zhensen Wu
CE0316	Adaptive Interleaving Method and its Application to Free Space Optical Communications through Atmospheric Turbulence Channel
	Zhonghua Yang, Qiwen Ran, Jing Ma, Liying Tan, Shichen Wu, Qingfeng liu, Huixi Liao

18：00 - 19：30	**Buffet Dinner**

Multi-Point Correction Method in CMOS Current-Mode Function Design

Kuo-Jen Lin
Department of Electronics Engineering
Chung Hua University
Hsinchu, Taiwan
Email: kuojenlin@chu.edu.tw

Chih-Jen Cheng and Jwu-E Chen
Department of Electrical Engineering
National Central University
Taoyuan, Taiwan
Email: 985401005@cc.ncu.edu.tw

***Abstract*—We propose a multi-point correction method to design a CMOS current-mode function with high input dynamic range. The dynamic range is dependent on the number of correcting circuits. Consider the accuracy, we can properly select the turn-on current in the correcting circuit. The exponential circuit for a design example, equipped with six correcting circuits, has a linearity of $39.5dB$ for linearity error less than 0.3 dB and has a large input dynamic range from $-60\mu A$ to $128\mu A$.**

I. Introduction

CMOS current-mode circuits are now attracting more attention in analog circuit design for their bandwidth, large dynamic range, and simplified circuitry. Most of CMOS current-mode circuits operate in the saturation region for high speed applications [1]–[10]. In the region, the square law characteristic of a MOS can be applied to design different functions such as exponential circuits [1]–[3], [5], geometric-mean circuits [4], [6], squarer/divider circuits [4], [6], square-rooter/multiplier circuits [6], [8], multiplier/divider circuits [4], [6], fuzzy logic circuit [6], gamma corrector [9], and fraction power circuits [3], [10].

For realizing some complex functions, several applications [2], [3], [5], [7], [9], [10] also use the second-order Taylor's approximations to approach the functions. However, the input dynamic range of the second-order Taylor's approximations are limited for required linearity and accuracy. Moreover, CMOS current-mode circuits suffer from the inherent second-order effects for only using the square-law approaches [4], [8]–[10].

Therefore, how to improve the accuracy and increase the input dynamic range are expected. In this paper, we propose a multi-point correction method to improve the weakness of designing a CMOS current-mode function.

II. Current-Mode Function Design

A. Quadratic Function

A quadratic circuit is shown in Fig. 1, which is constructed by the back-to-back connection of M1 and M2 [1]. Assuming that M1 and M2 are operating in the saturation region, then the MOS square-law describes the M1 and M2 drain currents:

$$I_1 = K_p(V_{gs} - |V_{tp}|)^2 = K_p(V_{DD} - V_c - |V_{tp}|)^2 \quad (1)$$

$$I_2 = K_n(V_{gs} - V_{tn})^2 = K_n(V_c - V_{tn})^2 \quad (2)$$

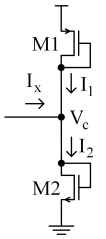

Fig. 1. Basic circuit.

where the transconductance parameters for M1 and M2 are: $K_p = \frac{1}{2}\mu_p C_{ox} W_1/L_1$ and $K_n = \frac{1}{2}\mu_n C_{ox} W_2/L_2$ respectively. Since $I_x = I_2 - I_1$, when $K = K_p = K_n$, we can derive V_c:

$$V_c = \frac{V_{DD} - |V_{tp}| + V_{tn}}{2} + \frac{I_x}{2K(V_{DD} - |V_{tp}| - V_{tn})} \quad (3)$$

Substituting (3) into (1) and (2) gives:

$$I_1 = K(\frac{V_{DD} - |V_{tp}| - V_{tn}}{2} - \frac{I_x}{2K(V_{DD} - |V_{tp}| - V_{tn})})^2 \quad (4)$$

$$I_2 = K(\frac{V_{DD} - |V_{tp}| - V_{tn}}{2} + \frac{I_x}{2K(V_{DD} - |V_{tp}| - V_{tn})})^2 \quad (5)$$

If we set $V_0 = \frac{V_{DD} - |V_{tp}| - V_{tn}}{2}$, then

$$I_1 = KV_0^2(1 - \frac{I_x}{4KV_0^2})^2 \quad (6)$$

$$I_2 = KV_0^2(1 + \frac{I_x}{4KV_0^2})^2 \quad (7)$$

We observe that I_1 and I_2 are the quadratic functions of I_x, which means the basic circuit is a current-mode quadratic circuit. To guarantee that M1 and M2 operate in the saturation region, the simple constrains are $V_c > V_{tn}$ and $V_{DD} - V_c > |V_{tp}|$. Therefore, from (3) we have $I_x > -4KV_0^2$ and $I_x < 4KV_0^2$.

B. Design Example

We design an exponential function for presentation. In order to reduce the circuit complexity, we approximate an exponential function using a second order Taylor polynomial.

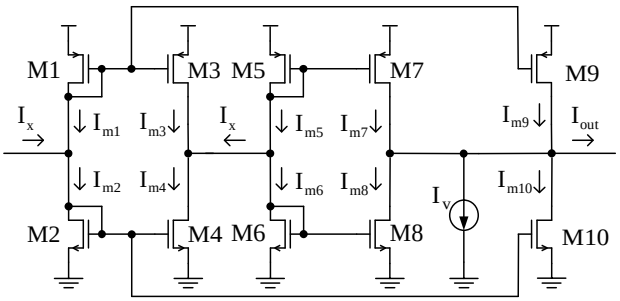

Fig. 2. Current-mode exponential circuit.

The second order polynomial for evaluating $\exp(x)$ at $x = 0$ is:

$$\exp(x) \approx 1 + x + \frac{1}{2}x^2 \tag{8}$$

Assume that $I_0 = KV_0^2$ and $I_x = I_0 x$. Equation (6) will be

$$I_1 = I_0(1 - \frac{x}{4})^2 \tag{9}$$

and (7) will be

$$I_2 = I_0(1 + \frac{x}{4})^2 \tag{10}$$

To realize the $exp(x)$ by using the current-mode circuit shown in Fig. 2, we could set the possible output (I_{out}) as

$$I_0 exp(x) = I_0(1 + x + \frac{1}{2}x^2) \tag{11}$$

We can rewrite it as

$$I_0 exp(x) = 8I_0(1 + \frac{x}{4})^2 - 3I_x - 7I_0 \tag{12}$$

or

$$\frac{I_0}{8} exp(x) = I_0((1 + \frac{x}{4})^2 + x) - \frac{11}{8}I_x - \frac{7}{8}I_0 \tag{13}$$

where $I_0((1 + \frac{x}{4})^2 + x)$ could be realized by

$$I_0((1 + \frac{x}{4})^2 + x) = 2I_0(1 + \frac{x}{4})^2 - I_0(1 - \frac{x}{4})^2 \tag{14}$$

which is the result of $(I_{m7} - I_{m8})$ as $I_{m7} = 2I_0(1 + \frac{x}{4})^2$ and $I_{m8} = I_0(1 - \frac{x}{4})^2$. Therefore, we could take mirrors from I_{m5} and I_{m6} to I_{m7} and I_{m8} with scale two and one, respectively. If we take mirrors from I_{m1} and I_{m2} with scale $\frac{11}{8}$ to I_{m9} and I_{m10}, respectively, then we can realize

$$I_{m10} - I_{m9} = \frac{11}{8}I_x \tag{15}$$

because

$$\frac{11}{8}(I_0(1 + \frac{x}{4})^2 - I_0(1 - \frac{x}{4})^2) = \frac{11}{8}I_x \tag{16}$$

If I_v is set to $\frac{7}{8}I_0$, and $I_{out} = \frac{I_0}{8}g(x) = I_u g(x) \approx I_u e^x$, then (13) can be rewritten as

$$I_{out} = I_{m7} - I_{m8} + I_{m9} - I_{m10} - I_v \tag{17}$$

which is achieved in Fig. 2.

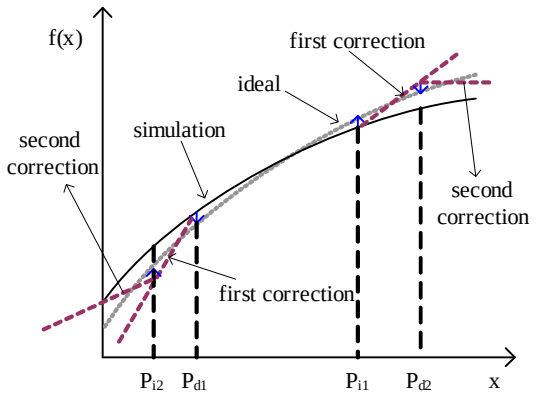

Fig. 3. Correcting points and their corrections.

III. Multi-Point Correction Method

In the previous circuit design, truncation errors are due to the Taylor's expansion; K-match errors are due to the assumption of (3); nonlinear errors are due to second-order effects such as channel length modulation, body effect, and mobility degradation. For reducing the errors, we could take some strategies as follows.

A. Sizing Strategy

We could tune the size of transistors which construct a current-mode function circuit to fit a function as possible. For example, we could size M3 and M4 in Fig. 2 to make the same value of two I_x. We can also tune the M7 and M8 to obtain a good result of $(I_{m7} - I_{m8})$, which could really match $I_0((1 + \frac{x}{4})^2 + x)$. We also size the M9 and M10 to realize (15). Consequently, we can accurately realize the Taylor's approximation circuit for the function of $\frac{I_0}{8}exp(x)$. However, the input dynamic range is also limited.

B. Multi-Point Correcting Circuit

In the design stage, simulation results could show the error figures. We could arrange some correcting points to correct errors. Figure 3 shows the error and correction examples. As $x > P_{i1}$ shown in Fig. 3, we could conduct P_{i1} circuit to increase the output current. As $x > P_{d2}$, we conduct P_{d2} circuit to decrease the output current. As $x < P_{d1}$, we could conduct P_{d1} circuit to decrease the output current. As $x < P_{i2}$, we conduct P_{i2} circuit to increase the output current. The P_{i1}, P_{d2}, P_{d1}, and P_{i2} circuits are shown in Fig. 4.

Consider accuracy and the input dynamic range, we need carefully tune the scales of current-mirrors of the correcting circuits. By using the multi-point correcting circuits, we can re-design the circuit shown in Fig. 2 into the circuit shown in Fig. 5. In Fig. 5, three P_{i1} circuits are used for $I_x > 0$ and two P_{d2} circuits and one P_{i1} circuit are used for $I_x < 0$. The number of correcting circuits is dependent on the accuracy and the input dynamic range.

IV. Simulation Results

To verify the sizing strategy and multi-point correcting circuit, we initiate a simulation by using the 0.35 μm CMOS

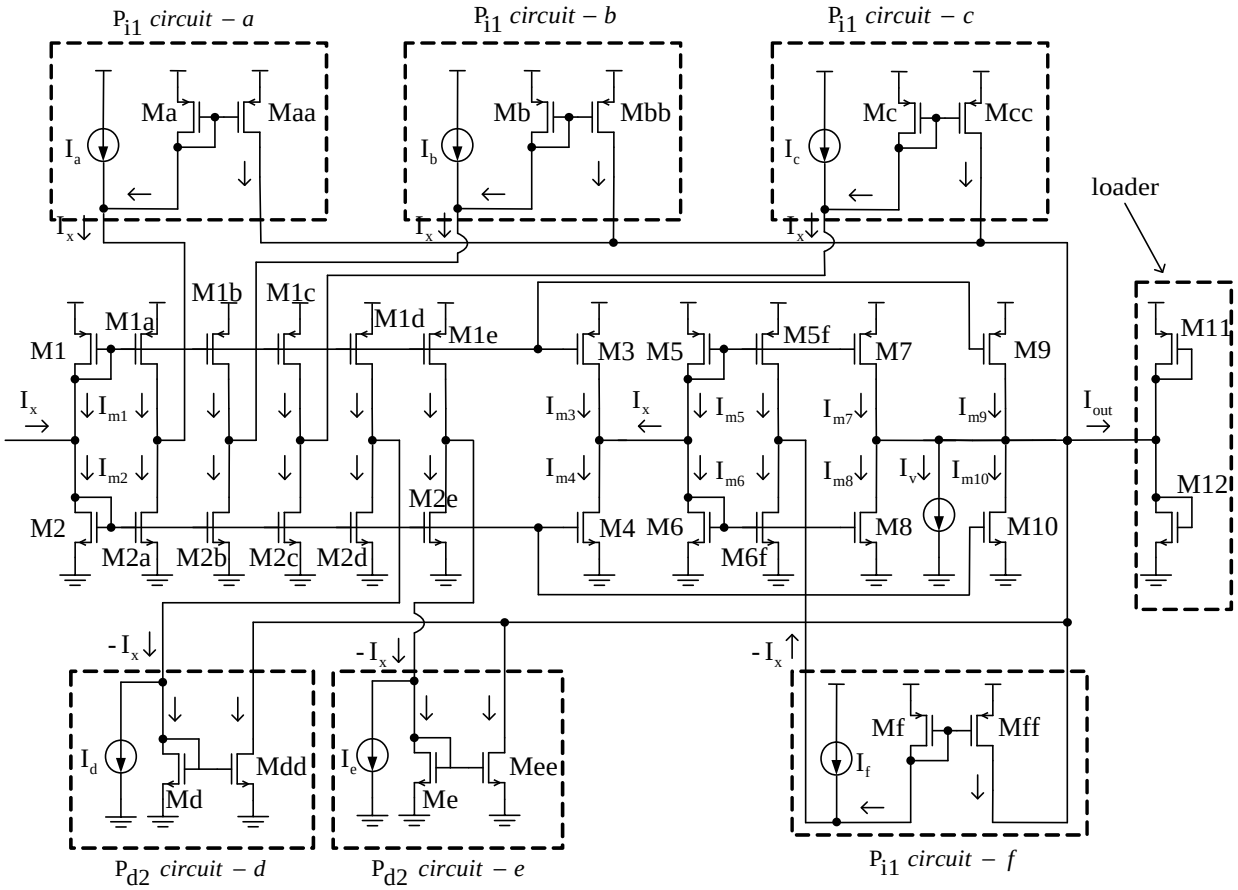

Fig. 5. Multi-point correction circuit for design example.

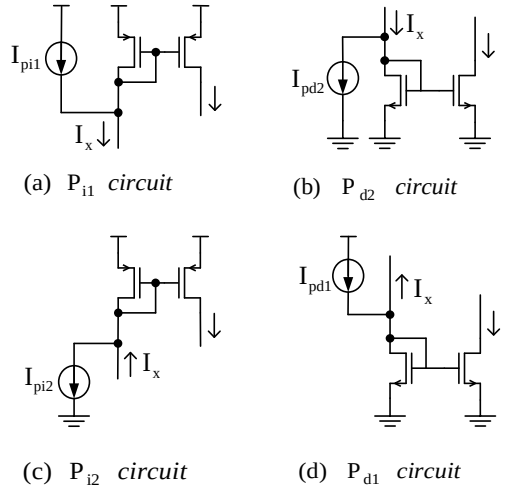

Fig. 4. Four different correcting circuits.

TSMC technology. The supply voltage V_{DD} of the circuit in Fig. 5 is set to be $2.5V$. If I_x is from $-120\mu A$ to $120\mu A$, then I_0 should be set to be $40\mu A$ for comparing to the input dynamic range from $x = -3$ to $x = 3$. Since the desired middle value of the input current range is $0\mu A$, the width of M5 and M6 is designed to be $3.5\mu m$ and $1.3\mu m$, respectively for making $K_p = K_n = K$ at $I_x = 0\mu A$. Consequently, due to $I_0 = KV_0^2$, I_0 is tuned to be $41.1\mu A$.

Figure 6 shows the I_{out} simulation results. The multi-point correction method nearly match the ideal exponential function for I_x from $-60\mu A$ to $128\mu A$. The linearity is about $39.5dB$ observed from Fig. 7 for linearity error less than $0.3dB$ shown in Fig. 8. The linearity of Taylor approximation is only $9dB$. From Fig. 8, we can observe that the correction points are located at $I_x = 18\mu A$, $I_x = 57\mu A$, $I_x = 93\mu A$, $I_x = -30\mu A$, $I_x = -53\mu A$, and $I_x = -57\mu A$. When $I_x = 18\mu A$, the P_{i1} circuit-a is on for $I_a = 18\mu A$, which controls the linearity error below 0.3 dB. Similarly, $I_b = 57\mu A$ and $I_c = 93\mu A$ for P_{i1} circuit-b and P_{i1} circuit-c, respectively. When $I_x = -30\mu A$ and $I_x = -53\mu A$, P_{d2} circuit-d and P_{d2} circuit-e are on for $I_d = 30\mu A$ and $I_e = 53\mu A$, which control the linearity error less than -0.3 dB. When $I_x = -57\mu A$, the P_{i1} circuit-f is on for $I_f = 57\mu A$, which controls the linearity error less than -0.3 dB. Obviously, the most efficient correction points for the exponential function design are located in the side of $I_x > 17\mu A$. This side contributes the input range from $17\mu A$ to $128\mu A$. On average,

TABLE I
EXPONENTIAL CIRCUIT COMPARISONS.

	Liu et al. [5]	Kumngern et al. [7]	Kalenteridis et al. [11]	proposed circuit
CMOS technology	$0.5\mu m$	$0.5\mu m$	$90nm$	$0.35\mu m$
Supply voltage	$\pm 2.5V$	1.5V	1.2V	2.5V
Linearity	15 dB	16.3 dB	17 dB	39.5 dB
Input dynamic range	-0.5V to 0.85V	$-11\mu A$ to $6.3\mu A$	-0.27V to 0.1V	$-60\mu A$ to $128\mu A$
Linearity error	1.35%	1 dB	0.5 dB	0.3 dB
Bandwidth	111.2 MHz		265 MHz	288 MHz

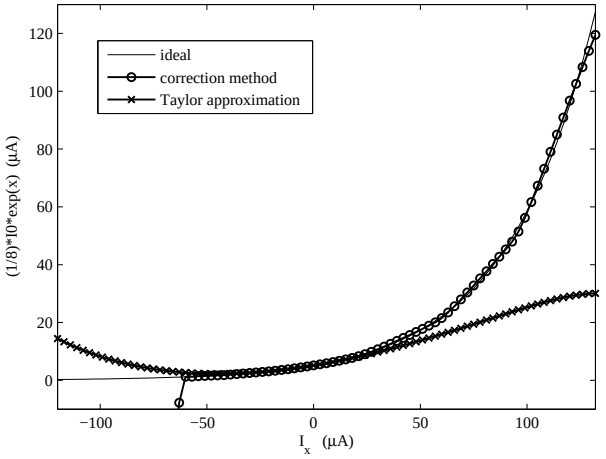

Fig. 6. Simulation results for $I_{out} = \frac{I_0}{8} exp(x)$.

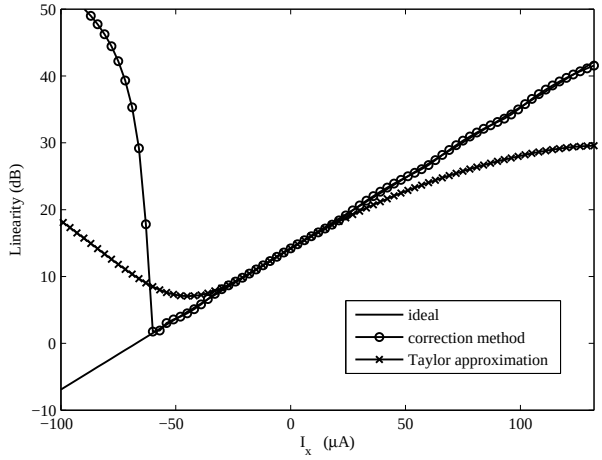

Fig. 7. Linearity measurements for correction method and Taylor's approximation.

each correcting circuit, constructed by four transistors and one current source, contributes $37\mu A$. Conversely, the other side only contributes the input range from $-60\mu A$ to $-28\mu A$. Each correcting circuit only contributes $11\mu A$ on average. The comparisons of relative circuits are given in Table I. Our proposed method and [7] adopt current-mode circuit, whereas [5] and [11] design circuits with voltage-mode. In [7] and [11], low voltage designs are with attraction. Our proposed circuit outperforms in linearity, input dynamic range, linearity error, and bandwidth.

V. CONCLUSION

In this paper, we propose a method to design a CMOS current-mode function with high input dynamic range. The sizing strategy contributes on correcting errors in the central part of a function. The proposed correcting circuits are used to extend the input dynamic range by decreasing errors from several correcting points. In the design example, we successfully implement an exponential function with a linearity of $39.5dB$ for an input range from $-60\mu A$ to $128\mu A$.

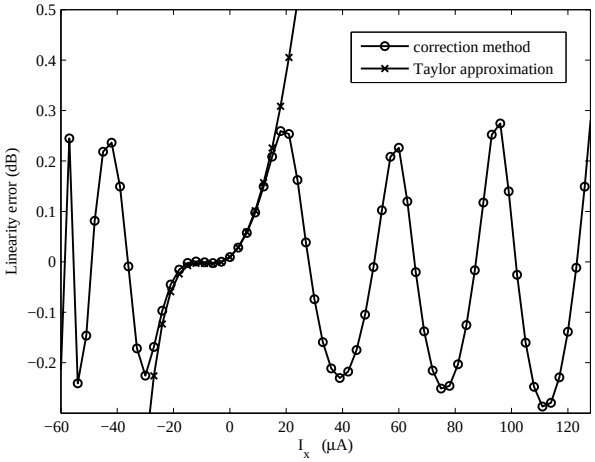

Fig. 8. Linearity errors for correction method and Taylor's approximation.

ACKNOWLEDGMENT

The authors would like to thank the National Chip Implementation Center (CIC) of the National Applied Research Laboratories of Taiwan for technical support. The research is supported by the National Science Council of Taiwan, under Grant No. NSC100-2221-E-216-033.

REFERENCES

[1] A. Motamed, C. Hwang, and M. Ismail, "CMOS exponential current-to-voltage converter," Electron. Lett., vol. 33, pp. 9981000, 1997.
[2] C. A. De La Cruz-Blas, A. Lopez-Martin, and A. Carlosena, " Pseudo-exponential function for mosfets in saturation," IEEE Trans. Circuit Syst.-II, vol. 47, pp. 13181321, 2000.
[3] M. T. Abuelmaatti, "Universal CMOS current-mode analog function synthesizer," IEEE Trans. Circuit Syst.-I, vol. 49, pp. 14681474, 2002.
[4] C. A. De La Cruz-Blas, A. Lopez-Martin, and A. Carlosena, "1.5-v mos translinear loops with improved dynamic range and their applications to

current-mode signal processing," IEEE Trans. Circuit Syst.-II, vol. 50, pp. 918927, 2003.
[5] W. Liu, S. I. Liu, and S. K. Wei, " CMOS differential-mode exponential voltage-to-current converter," Analog Integrated Circuits and Signal Processing, vol. 45, pp. 163168, 2005.
[6] M. Mottaghi kashtiban, A. Khoei, and K. Hadidi, "A current mode, first-order Takagi-Sugeno-Kang fuzzy logic controller, supporting rational-powered membership functions," IEICE Trans. Electron, vol. E90-C, pp. 12581266, 2007.
[7] M. Kumngern, J. Chanwutitum, and K. Dejhan, "Simple CMOS current-mode exponential function generator circuit," Proceedings of ECTI-CON, Krabi, pp. 709712, 2008.
[8] J. K. Seon, "Design and application of precise analog computational circuits," Analog Integrated Circuits and Signal Processing, vol. 54, pp. 5566, 2008.
[9] K. J. Lin, C. J. Cheng, H. C. Su, and B. Yu, "Design of CMOS current-controlled-gamma corrector," Int. J. Electron. Commun. (AEU), vol. 65, pp. 9971005, 2011.
[10] K. J. Lin, C. J. Cheng, S. F. Chiu, and H. C. Su, "CMOS current-mode implementation of fractional-power functions," Circuits, Systems, and Signal Processing, vol. 31, pp. 61-75, 2012.
[11] V. Kalenteridis, S. Vlassis, and S. Siskos, "A CMOS linear-in-dB VGA based on exponential current generator," 6th International Conference on Design & Technology of Integrated Systems in Nanoscale Era, Athens, pp. 14, 2011.

ICEOE2012 and OEMR2012 CONFERENCES SCHEDULE

2012 2nd International Conference on Electronics and Optoelectronics (ICEOE 2012)

2012 International Meeting on Opto-Electronics Engineering and Materials Research (OEMR 2012)

Tianlun Regar Hotel Shenyang

Shenyang, China

July 27 - 28, 2012

July 27, 2012 (Friday)

Lobby of Tianlun Regar Hotel Shenyang (沈阳天伦瑞格酒店大厅)

10：00 – 12：00 14：30 – 18：00	Arrival and Registration

Note：(1) You can also register at any time during the conference.

(2) Certificate of Participation can be collected at the registration counter.

(3) The organizer won't provide accommodation, and we suggest you make an early reservation.

Morning, July 28, 2012 (Saturday)

RUIHE A Hall of The Sixth Floor

6 层瑞和 A 厅

Time: 9:00-12:00

OE0150	Characteristic of Point Defect around the Photonic Crystal Bend
	Ruei-Chang Lu, Chun-Min Wang and Keh-Yi Lee
OE0151	Wavelength Division Multiplexer based on Periodic Dielectric Waveguide Ring Resonator
	Ruei-Chang Lu, Tung-Hao Chen and Yu-Ping Lia
OE0800	A new design of large area MCP-PMT for the next generation neutrino experiments
	Sen. Qian
OE0183	Noise Analysis of EMCCD and Optimum Design of Its Operating Mode
	Yugui Zhang,Tao Li and Zhikuan He
OE0590	Optimal Design of CCD Driving Signal Based on FLEX 10K
	Zhikuan He, Songbo Wu and Yugui Zhang
OE0239	A 5-port Photonic Lantern for Light Beam Combining
	Yan Qi, Haijiao Yu,Fengjun Tian and Weimin Sun
OE0539	CPU Experiment of Heat Dissipation and Temperature Rise
	Maode Li,Wei Wei and Yi Li
OE0235	Influence of Pump Light's Duty Cycle on Cesium Atomic Magnetometer
	Xianjin Zeng, Junhai Zhang, Qiang Liu, Zongjun Huang and Weimin Sun
OE0645	Influence of Plasmonic Light-Scattering by Gold Nano-island Structures on the Quantum Efficiency of Organic Solar Cell
	Baozeng Wang,Xinping Zhang and Jian Zhang
OE0646	Directly-Written Metallic Photonic Crystals for Sensor Applications
	Jian Zhang,Xinping Zhang,Zhaoguang Pang and Baozeng Wang
OE0195	The Effects of Pump Beam on Cesium Magnetometer Sensitivity
	Qingmeng Li, Qiang Liu, Junhai Zhang, Zongjun Huang, Xianjin Zeng and Weimin Sun
OE0584	Measurement of SO2 using Differential Optical Absorption Spectroscopy
	Haiming Zheng, Zhenliang Dong, Dongshui Xie and Xiaoxiao Shang

OE0109	Study On Control Technology of Double-fed Motor Based On PLC and General Invert
	Chengwu Lin, Jialin Shi and Bo Lu
OE0110	Research on Grid-connected Inverter Based on Current Track Control in Wind Generation System
	Chengwu Lin, Qiguang Jiang and Li Ma
OE0568	A new Coupled PDE Method for Image Processing
	Maolin Wang, Jun Yue, Pan Huang and Chaoshuai Song
OE0214	Comparison of Gold and Silver Nanoparticles as Active Substrates for SERS Spectra Measurements on Liver Cancer Cells
	Chen Qian,Shupeng Liu,Na Chen,Zhenyi Chen and Qianqian Geng
OE0202	Generation of Multi-Atom W States in Microtoroidal Cavity-Atom System
	Yu Huang
OE0165	A Method for Lidar Data Conversion and Standardization
	Hao Chen, Dengxin Hua, Yikun Zhang, Zhirong Zhou, Shichun Li and Li Wang
OE0233	The structural design of combined absorber composed by MPP and multi-layer porous material based on VA One
	Xiuhua Duan, Huanqin Wang,Wenjuan Sun and Deyi Kong
OE0537	Studying Relative Error Formulae of Surveying Textbooks of Chinese Colleges
	Yonghe Deng
OE0245	Dynamically manipulating beam with metallic nano-optic lens containing liquid crystal
	Jicheng Wang, Xia Zhou,Jie Gao,Zhetao Xu, Lin Sun and Xiao Jin
OE0550	Solvothermal method preparation of nano Y2O2SEu3+ and research of luminescence property
	Lu Lu and Zhilong Wang

12：00 - 13：30	Lunch Break

Afternoon, July 28, 2012 (Saturday)

RUIHE A Hall of The Sixth Floor

6 层瑞和 A 厅

Time: 14:00-18:00

CE0105	Fault diagnosis of COIL based on BP Artificial Neural Network
	Zheng Zhang, Shiqiang Zhang, Yanhong Sun
CE0121	Study of Top Triangular Nano-grating on Solar Cell Using Rigorous Coupled Wave Analysisg
	Xiaomin Jin, Douglas Alan Cattarusa, and Michael James Marshall
CE0126	Comparative Research on Different Solutions of a High-Performance Thin-Film Polarizing Beam Splitter
	Kaiyong Yang, Hongchang Zhao, Yunfeng Jia, Suyong Wu
CE0140	Optimization Of Fiber Length For Edfa To Enhance The Channel Capacity Of Dwdm System
	Inderpreet Kaur, Neena Gupta
CE0143	Long-haul Wavelength Division Multiplexing Secure Communications with Chaotic Optical Channels
	Xiaolei Chen, Qingchun Zhao, Hongxi Yin, Xinyu Dou
CE0145	Optical-Mode Study of Galium Nitrate Based Laser Diodes
	Douglas Alan Cattarusa, Xiaomin Jin, Xiao-Hua Yu, Xing-Xing Fu, Xiang-Ning Kang, Bei Zhang, Guo-Yi Zhang
CE0157	A simple mechanism to suppress the mode competition for stable and tunable dual-wavelength erbium-doped fiber lasers
	Chenfang Zhang, Jiang Sun, Siwen Zheng and Shuisheng Jian
CE0166	Application of Optical Phase conjugation in Adaptive optics to remove atmospheric aberrations from an optical wavefront
	Sriram Rengarajan, Nandhakishore Perarulalan
CE0172	Study on Optical Performance Monitoring for Fiber-optical Link Utilizing Chaos Theory
	Qingqing Fan, He Li, Hongxi Yin
CE0186	Multi-Point Correction Method in CMOS Current-Mode Function Design
	Kuo-Jen Lin, Chih-Jen Cheng, Jwu-E Chen
CE0199	CMOS Current-Mode Hyperbolic Tangent Sigmoid Function Implementation Using Multi-Segment Approximations
	Chih-Jen Cheng, Kuo-Jen Lin, Jwu-E Chen
CE0235	The development of Remote Measurement System Based on GSM Internet of Things(IOT)
	Yunxin Gong, Houyu Zhao
CE0245	Research of Temperature Compensation for Ultrasonic Rangefinder
	Gang Tian, Jun Gui
CE0247	Analysis on the Relationship Between Burst Errors and Tracking Control Frequency in Satellite-to-Ground Laser communications
	Qiwen Ran, Zhonghua Yang, Jing Ma, Liying Tan, Shichen Wu, Qingfeng liu, Huixi

	Liao
CE0273	The three-dimensional analysis of light scattering characters for Rayleigh particles on/below the wafer
	Lei Gong, Zhensen Wu
CE0282	Simulation of Laser Beam Scattering from Complex Targets in the Near Field
	Jiaxuan Lin, Zhensen Wu, Xiang Su, Biao Wang
CE0284	The Analysis of Influencing Factors of One Dimensional Range Profiles and Surface Elements Imaging Method to Arbitrary Target
	Yuan Mou, Zhensen Wu, Zhuo Chen, Hanlu Zhang
CE0285	Scattering Properties of the Higher-Order Hermite Gaussian Beam
	Tan Qu, Zhensen Wu, Haiying Li, Zhengjun Li
CE0287	Extraordinary Electromagnetic Scattering of Plane Wave by Double Negative Coated Sphere
	Yan'e Shi, Zhensen Wu, Hongfei Tian, Zhengjun Li
CE0288	Scattering Characteristics of Complex Target from Solar Irradiance and Sky-ground Background Radiance in Infrared Spectrum
	Xing Guo, Zhensen Wu, Longxiang Linghu, Yufeng Yang
CE0289	Scattering of Two-Dimensional Sea Surface at Low Grazing Angles with Physical Optics Method
	Zhuo Chen, Zhensen Wu, Yong Zhang, Jingjing Xue, Wenhua Ye
CE0292	The Acceleration of PO Based on CUDA
	Xiang Su, Zhensen Wu, Jiaxuan Lin and Xiaobing Wang
CE0293	Decomposing the Non-Gaussian Surface in Sum of Gaussian Surfaces
	Zhangxing Qi, Zhensen Wu, Ziwen Yu, Haiying Li
CE0294	Polarization Properties of Scattered Fields from a Chiral Sphere
	Qingchao Shang, Zhensen Wu, Peng Zhao, Zhengjun Li
CE0311	Phase-only Beam Optimization for GaAs Optical Waveguide Phase Array
	Yong Zhang
CE0314	Path loss of Non-Line-of-Sight single-scatter model
	Tairong Wang, Lu Bai, Zhensen Wu
CE0316	Adaptive Interleaving Method and its Application to Free Space Optical Communications through Atmospheric Turbulence Channel
	Zhonghua Yang, Qiwen Ran, Jing Ma, Liying Tan, Shichen Wu, Qingfeng liu, Huixi Liao

18：00 - 19：30	**Buffet Dinner**

CMOS Current-Mode Hyperbolic Tangent Sigmoid Function Implementation Using Multi-Segment Approximations

Chih-Jen Cheng
Department of Electrical Engineering
National Central University
Taoyuan, Taiwan
Email: 985401005@cc.ncu.edu.tw

Kuo-Jen Lin (corresponding author)
Department of Electronics Engineering
Chung Hua University
Hsinchu, Taiwan
Email: kuojenlin@chu.edu.tw

Jwu-E Chen
Department of Electrical Engineering
National Central University
Taoyuan, Taiwan
Email: jechen@ee.ncu.edu.tw

***Abstract*—We propose a multi-segment approximation method to design a CMOS current-mode hyperbolic tangent sigmoid function with high accuracy and wide input dynamic range. The dynamic range is dependent on the number of segments and the accuracy is related to the dividing point. From mathematical results, we can observe the proposed method outperforms traditional methods. We implement the multi-segment approximation circuit to realize the hyperbolic tangent sigmoid function. The simulation results of the proposed circuit show a wide input dynamic range from $-256\mu A$ to $240\mu A$ for relative error less than 3% and a high bandwidth of 138 MHz.**

I. Introduction

In the era of increasingly sophisticated electronic technology, to handle complicated applications often must rely on more complicated functions to assist in the circuit design. The hyperbolic tangent sigmoid function (tanh), which is used as the transfer function of the artificial neural network (ANN) for the input layer and the hidden layer. In the previous literature, the tanh function is designed by using digital circuits [1], [2], which occupy a large area and high power consumption. In [3], authors implement the tanh function by using analog circuits, which are composed of CMOS circuits operated in weak inversion. However, the speed, input dynamic range, and accuracy for these applications are limited. For improving the speed and the total harmonic distortion (THD), Berg et al. proposed a floating gate CMOS to implement the tanh function [4]. CMOS current-mode circuit naturally becomes the most favorable circuit. Most of CMOS current-mode circuits operate in the saturation region for high speed applications [5]–[7]. In the region, the square law characteristic of a MOS can be applied to design different functions such as exponential circuits [6], [8], geometric-mean circuits [5], [7], and fuzzy logic circuit [7]. Several applications [6], [8], [9] also use the second-order Taylor's approximations to approach the functions. However, the input dynamic range of the second-order Taylor's approximations are also limited for accuracy requirement.

In this paper, we propose a multi-segment approximation circuit to realize a tanh function with the characteristics of high speed, wider input dynamic range, and high accuracy. We divide the function into four segments. Each segment, we use the quadratic polynomial approach to reduce the complexity of the circuit. The dividing point should be dependent on the required accuracy. The number of segments should relate to the input dynamic range.

II. Multi-Segment Approximation Method

The sigmoid function is non-linear, continuous, and differentiable, allowing it to map complex relations and provide a closed form when weights are updated during training of the neural network [10]. The tanh(x) could be approximated by Taylor's series for the expansion point at $x = 0$:

$$tanh(x) = x - \frac{x^3}{3} + \frac{2x^5}{15} - \frac{17x^7}{315} + \cdots \quad (1)$$

In Eq. (1), the x^3, x^5, and even x^7 are very difficult to implement by using CMOS current-mode circuits. Therefore, we divide the $tanh(x)$ into four segments which could be realized by second-order polynomials. We need to re-expand the $tanh(x)$ at different points a_i, the middle value of segment i, for using the Taylor's series:

$$tanh_i(x) \approx p_i x^2 + q_i x + r_i \quad (2)$$

where $p_i = -sech^2(a_i)tanh(a_i)$, $q_i = sech^2(a_i) - 2a_i p_i$, and $r_i = tanh(a_i) - a_i sech^2(a_i) + a_i^2 p_i$. When we select $a_1 = -1.68$, $a_2 = -0.56$, $a_3 = 0.56$, and $a_4 = 1.68$, we could approximate the $tanh_i(x)$ for different x intervals, respectively:

$$tanh_1(x) \approx 0.121x^2 + 0.537x - 0.373 \quad (x < -1.2) \quad (3)$$

$$tanh_2(x) \approx 0.377x^2 + 1.164x + 0.026 \quad (-1.2 \le x < 0) \quad (4)$$

$$tanh_3(x) \approx -0.377x^2 + 1.164x - 0.026 \quad (0 \le x < 1.2) \quad (5)$$

$$tanh_4(x) \approx -0.121x^2 + 0.537x + 0.373 \quad (x \ge 1.2) \quad (6)$$

Mathematical simulation results are shown in Fig. 1 for the four segmented approaches. For relative error less than 3%, the traditional Taylor's methods of expansion to the terms of x^3 , x^5, and x^7 have the input dynamic ranges of 1.3, 1.7, and

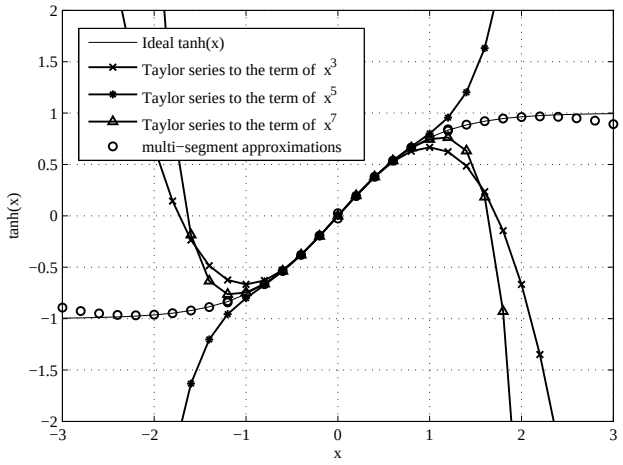

Fig. 1. Mathematical simulation results for different approximations.

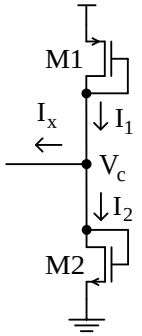

Fig. 2. Simple current-mode quadratic circuit.

2.0, respectively. The proposed multi-segment approximation reveals the wide input dynamic range of 5 for relative error less than 3%. Obviously, our proposed method outperforms the traditional methods.

III. Multi-Segment Approximation Circuit

The simulation result of Fig. 1 gives the good way to implement the tanh function by using four second-order polynomial functions. We will illustrate how to realize and control the four segments by using CMOS current-mode circuits.

A. Quadratic Circuit

We can generate a current-mode quadratic function by using a simple circuit shown in Fig. 2 [11]. From [12], we have two current-mode functions:

$$I_1 = K(\frac{V_{DD}-|V_{tp}|-V_{tn}}{2} + \frac{I_x}{2K(V_{DD}-|V_{tp}|-V_{tn})})^2 \quad (7)$$

$$I_2 = K(\frac{V_{DD}-|V_{tp}|-V_{tn}}{2} - \frac{I_x}{2K(V_{DD}-|V_{tp}|-V_{tn})})^2 \quad (8)$$

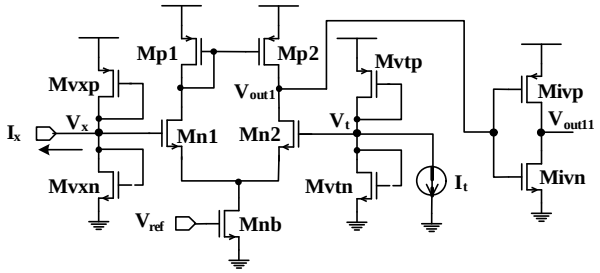

Fig. 3. Segment controller.

and

$$V_c = \frac{V_{DD}-|V_{tp}|+V_{tn}}{2} - \frac{I_x}{2K(V_{DD}-|V_{tp}|-V_{tn})} \quad (9)$$

Obviously, I_1 and I_2 are the quadratic functions of I_x. As I_x increases, V_c will decrease for observing Eq. (9). If we set $V_0 = \frac{V_{DD}-|V_{tp}|-V_{tn}}{2}$, then

$$I_1 = KV_0^2(1+\frac{I_x}{4KV_0^2})^2 \quad (10)$$

$$I_2 = KV_0^2(1-\frac{I_x}{4KV_0^2})^2 \quad (11)$$

If we set $I_0 = KV_0^2$ and $I_x = 4I_0x$. Equation (10) will be

$$I_1 = I_0(1+x)^2 \quad (12)$$

and (11) will be

$$I_2 = I_0(1-x)^2 \quad (13)$$

B. Segment Controller

We need to design a control circuit to switch the services of Eqs. (3), (4), (5), and (6). Therefore, we could design the segment controller shown in Fig. 3 based on a differential amplifier. If $I_x > I_t$, we have $V_x < V_t$, which make V_{out1} near ground (GND) and V_{out11} near VDD. Conversely, if $I_x < I_t$, we have the results of V_{out1} near VDD and V_{out11} near GND. For controlling four segments ($s1$, $s2$, $s3$, and $s4$), we need to construct a four-segments controller shown in Fig. 4. The V_{out1}, V_{out2}, and V_{out3} are controlled by I_{t1}, I_{t2}, and I_{t3}, respectively. A corresponding control table is shown in Table I.

In Fig. 4, the $s1$, $s2$, $s3$, and $s4$ segment circuits realize the Eqs. (3), (4), (5), and (6), respectively. The drain current of Mep12 is the scale of $I_0(1+x)^2$, we could size Mep12 and tune I_{b1} to make $I_0tanh_1(x)$ shown in Eq. (3). The $s2$ segment circuit also follows the sizing and tuning method. The $s3$ and $s4$ segment circuits will have $I_0tanh_3(x)$ and $I_0tanh_4(x)$. The $I_0tanh_3(x)$ is made by $AI_0(1+x)^2 - BI_0(1-x)^2$, where A and B are the scale of Mep32 and Men32, respectively, which are determined by Eq. (5) and tuned by observing the results of simulation. The similar work should apply on the generation of $I_0tanh_4(x)$.

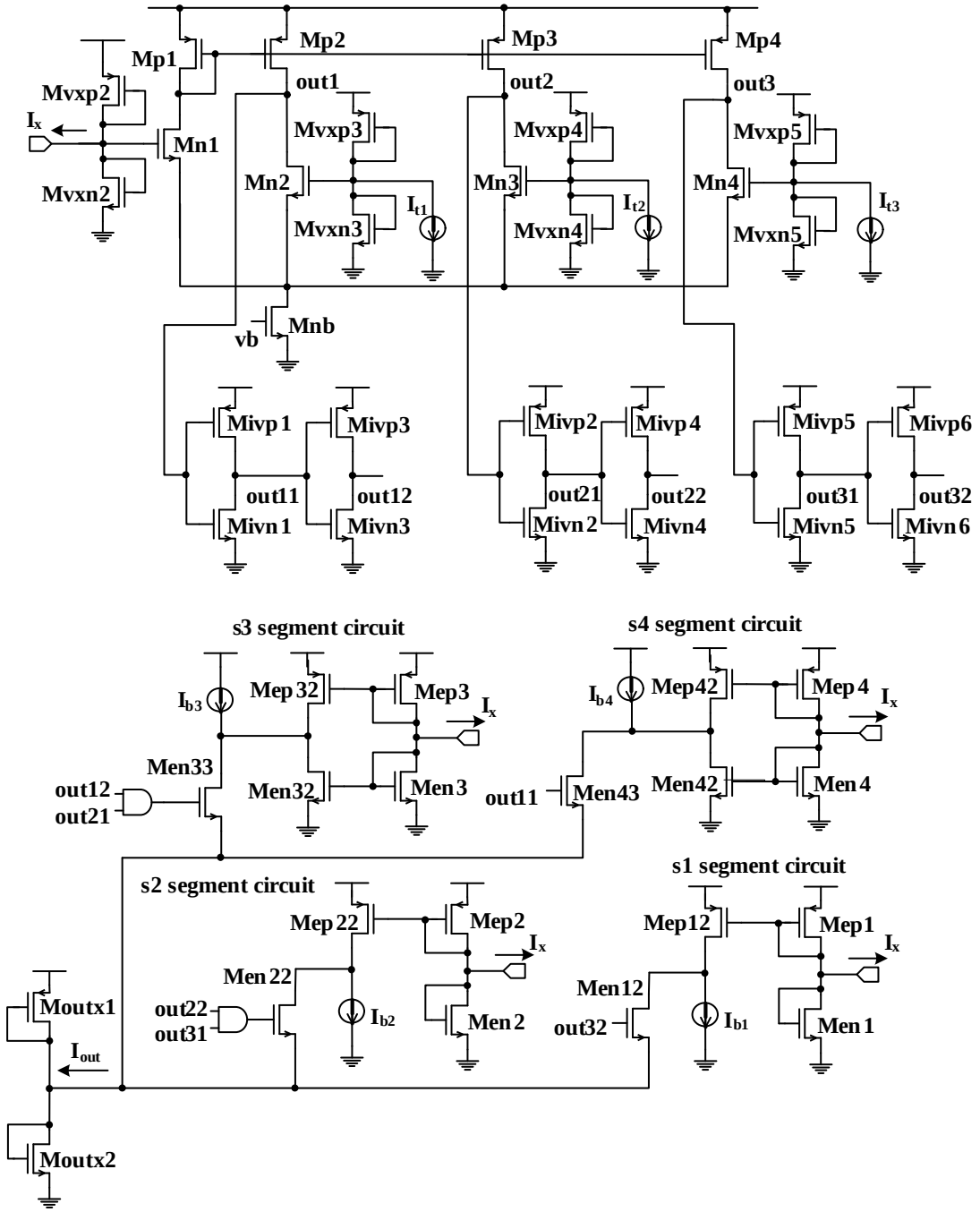

Fig. 4. Multi-segment approximation circuit for tanh.

IV. Simulation Results

To verify the multi-segment approximation circuit, we initiate a simulation by using the 0.35 μm CMOS TSMC technology. The supply voltage V_{DD} of the circuit in Fig. 4 is set to be $2.5V$. When we set $I_0 = 30\mu A$, we can observe I_x from $-300\mu A$ to $300\mu A$ for input dynamic range from $x = -2.5$ to $x = 2.5$. Figure 5 shows the I_{out} simulation results. The multi-segment approximation method nearly match the ideal tanh function for I_x from $-256\mu A$ to $240\mu A$ with relative error less than 3%. This range is mapped to x from -2.13 to 2.0. The total input dynamic range is about 4.13. The measured frequency response of I_{out} is shown in Fig. 6. The $-3dB$ bandwidth is 138 MHz. The THD measurements of I_{out} are shown in Fig. 7 for input DC current of $30\mu A$ and $130\mu A$ with sinusoidal signals of amplitude I_a from $2\mu A$ to $20\mu A$ at the frequency of 100 KHz.

V. Conclusion

In this paper, we propose a multi-segment method to design a CMOS current-mode hyperbolic tangent sigmoid function.

TABLE I
FOUR-SEGMENTS CONTROL TABLE.

Segment	s1 on $(I_x < I_{t3})$	s2 on $(I_{t3} \leq I_x < I_{t2})$	s3 on $(I_{t2} \leq I_x < I_{t1})$	s4 on $(I_x \geq I_{t1})$
V_{out11}	low	low	low	high
V_{out12}	high	high	high	low
V_{out21}	low	low	high	high
V_{out22}	high	high	low	low
V_{out31}	low	high	high	high
V_{out32}	high	low	low	low

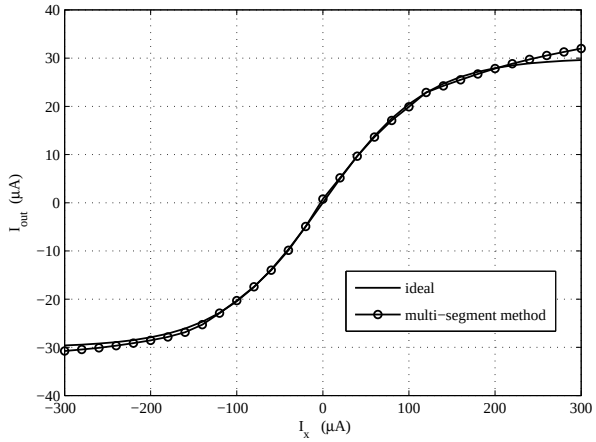

Fig. 5. Simulation results for current-mode tanh function.

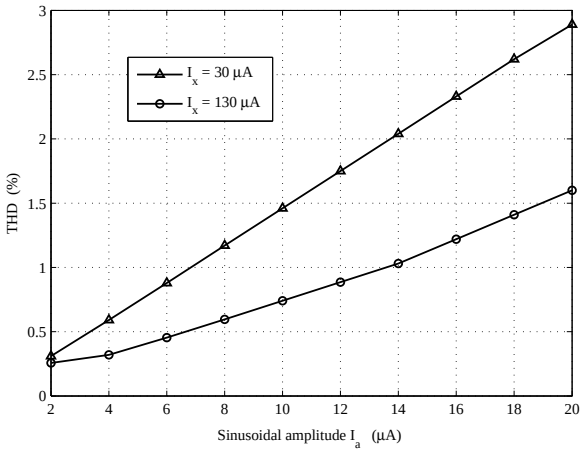

Fig. 7. THD measurement of the multi-segment approximation circuit.

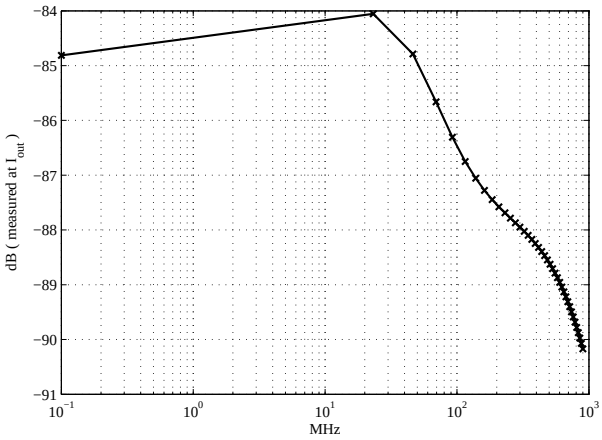

Fig. 6. Bandwidth measurement of the multi-segment approximation circuit.

The proposed multi-segment approximation circuit has been verified with wide input dynamic range from $-256\mu A$ to $240\mu A$ for relative error less than 3%, which is wider than the Taylor's method of expanding series to the term of x^7. Moreover, we measure $-3dB$ bandwidth of $138MHz$. The THD measurements are less than 2.9% for large sinusoid amplitude.

ACKNOWLEDGMENT

The authors would like to thank the National Chip Implementation Center (CIC) of the National Applied Research Laboratories of Taiwan for technical support. The research is supported by the National Science Council of Taiwan, under Grant No. NSC100-2221-E-216-033.

REFERENCES

[1] M. Skrbek, and M. Snorek, "Shift-add neural architecture," Proc. 6th IEE Int. Conference on Circuits and Systems, vol. 1, pp. 411-414, 1999.

[2] S. Marra, M. A. Iachino, and F. C. Morabito, "High speed, programmable implementation of a tanh-like activation function and its derivative for digital neural networks," Proceedings of International Joint Conference on Neural Networks, pp. 506-511, 2007.

[3] M. Carrasco-Robles and L. Serrano, "A novel CMOS current mode fully differential tanh(x) implementation," ISCAS, pp. 21582161, 2008.

[4] Y. Berg, S. Aunet, O. Naess, and M. Hovin, "A novel low-voltage floating-gate CMOS transconductance amplifier with sinh (tanh) shaped output current," The 8th IEEE International Conference on Electronics, Circuits and Systems, vol. 3, pp. 1461-1464, 2001.

[5] C. A. De La Cruz-Blas, A. Lopez-Martin, and A. Carlosena, "1.5-v mos translinear loops with improved dynamic range and their applications to current-mode signal processing," IEEE Trans. Circuit Syst.-II, vol. 50, pp. 918927, 2003.

[6] W. Liu, S. I. Liu, and S. K. Wei, " CMOS differential-mode exponential voltage-to-current converter," Analog Integrated Circuits and Signal Processing, vol. 45, pp. 163168, 2005.

[7] M. Mottaghi kashtiban, A. Khoei, and K. Hadidi, "A current mode, first-order Takagi-Sugeno-Kang fuzzy logic controller, supporting rational-powered membership functions," IEICE Trans. Electron, vol. E90-C, pp. 12581266, 2007.

[8] M. T. Abuelmaatti, "Universal CMOS current-mode analog function synthesizer," IEEE Trans. Circuit Syst.-I, vol. 49, pp. 14681474, 2002.
[9] M. Kumngern, J. Chanwutitum, and K. Dejhan, "Simple CMOS current-mode exponential function generator circuit," Proceedings of ECTI-CON, Krabi, pp. 709712, 2008.
[10] M. Akay, Nonlinear Biomedical Signal Processing, Fuzzy Logic, Neural Networks, and New Algorithms, 2000.
[11] A. Motamed, C. Hwang, and M. Ismail, "CMOS exponential current-to-voltage converter," Electron. Lett., vol. 33, pp. 9981000, 1997.
[12] K. J. Lin, C. J. Cheng, S. F. Chiu, and H. C. Su, "CMOS current-mode implementation of fractional-power functions," Circuits, Systems, and Signal Processing, vol. 31, pp. 61-75, 2012.

PAPER *Special Section on Electronic Displays*

A CMOS Current-Mode S-Shape Correction Circuit with Shape-Adjustable Control

Kuo-Jen LIN[†], ***Member***, **Chih-Jen CHENG**[††], **Hsin-Cheng SU**[†], ***and*** **Jwu-E CHEN**[††], ***Nonmembers***

SUMMARY A CMOS current-mode S-shape correction circuit with shape-adjustable control is proposed for suiting different LCD panel's characteristics from different manufactures. The correction shape is divided into three segments for easy curve-fitting using three lower order polynomials. Each segment could be realized by a corresponding current-mode circuit. The proposed circuit consists of several control points which are designed for tuning the correction shape. The S-shape correction circuit was fabricated using the 0.35 μm TSMC CMOS technology. The measured input dynamic range of the circuit is from 0 μA to 220 μA. The -3 dB bandwidth of the circuit is up to 262 MHz in a high input current region.

key words: *TFT-LCD, S-shape correction, current-mode circuit, quadratic circuit*

1. Introduction

In the past decade, with the rapid increase in mobile cameras, mobile phones can now capture and store still images or moving pictures as digital files. As a result, there is a significant difference in the color appearance when captured images are displayed on a mobile LCD. Therefore, real-time color-matching between mobile camera and mobile LCD in a mobile phone needs to be considered to ensure a better image quality [1], [2]. The color-correct visualizations of the LCD displays become more and more important.

The electro-optical transfer function of an LCD display is called S-shape curve. Previous works [3]–[6] used several resistors and operational amplifiers to construct different grey scale's voltage for correcting the S-shape. In [7], authors proposed an analog compensating S-shape circuit which is composed of BJTs. Comparing to [3]–[6], the technology in [7] is more suitable for mobile device due to the low circuit complexity. In [8], a new model was developed for the S-shaped electro-optical transfer function of the LCD device. However, due to different LCD panel's spectral and gamma characteristics at different manufacturers [9], one should make different corrections. In [10], a CMOS current-mode S-shape correction circuit with four selectable curves was proposed to meet for four corrections. The authors adopted a polynomial form to represent an S-shape and generated different shapes by adjusting two variables. However, the CMOS current-mode circuit, including a multiplier, a square circuit, and an approximation fractional-power circuit, has weaknesses in power, bandwidth, complexity, and curvature.

In this paper, we also use the CMOS current-mode circuits to design the S-shape correction function, because the current-mode circuit has the advantages of higher bandwidth, large dynamic range, and simplified circuitry. We divide a pseudo S-shape correction curve into three segments. Each segment has a corresponding circuit with adjustable control points. By adjusting the control points, we can obtain a suitable S-shape correction curve.

2. S-shape Correction Curves

A CRT display and an LCD display have electro-optical transfer functions shown in Fig. 1, where the transfer function of an LCD is an S-shaped curve. As same as the gamma correction curve shown in Fig. 1(a), Fig. 1(b) shows an S-shape correction curve. Because different manufacturers have different electro-optical characteristics, we can use Fig. 2(a) to show some examples of different electro-optical transfer functions. Similarly, Fig. 2(b) shows some examples of S-shape correction curves.

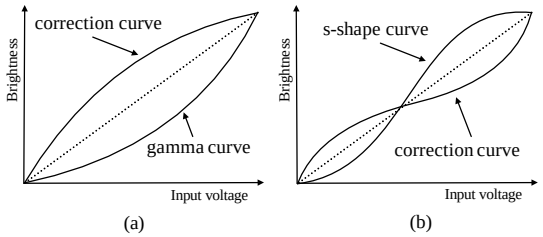

Fig. 1 (a) The electro-optical transfer function of a CRT display and its correction curve. (b) The electro-optical transfer function of an LCD display and its correction curve.

The curves shown in Fig. 2(b) are not mathematical functions, which are hard to describe by some polynomial approximations. We observe that these curves rise quickly on the high voltage part and low voltage part, but slowly on the middle voltage part. Hence, we can certainly divide the S-shape correction curves into three segments. Segment A, B, and C are corresponding to the curve on high, low, and middle voltage part, respectively. We observe that different curves have different segment-curvatures and segment-lengths. The curvature and length will be the important parameters for designing the circuit. Moreover, each segment

Manuscript received January 1, 2011.
Manuscript revised January 1, 2011.
[†]The authors are with the Department of Electronics Engineering, Chung Hua University, Hsinchu, Taiwan
[††]The authors are with the Department of Electrical Engineering, National Central University, Taoyuan, Taiwan
DOI: 10.1587/transele.E0.C.1

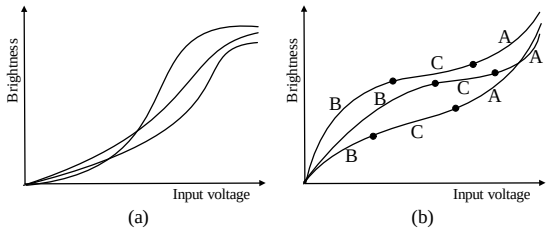

Fig. 2 (a) Different electro-optical characteristics for different LCD manufacturers. (b) Different S-shape correction curves for different LCD manufacturers.

could be approximated by using lower order polynomial due to low curvature.

3. Circuit Design and Simulations

We can generate a current-mode quadratic function by using a simple circuit shown in Fig. 3 [11]. From [10], we have

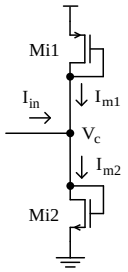

Fig. 3 Simple current-mode quadratic circuit.

two current-mode functions:

$$I_{m1} = K(\frac{V_{DD} - |V_{tp}| - V_{tn}}{2} - \frac{I_{in}}{2K(V_{DD} - |V_{tp}| - V_{tn})})^2 \quad (1)$$

$$I_{m2} = K(\frac{V_{DD} - |V_{tp}| - V_{tn}}{2} + \frac{I_{in}}{2K(V_{DD} - |V_{tp}| - V_{tn})})^2 \quad (2)$$

Obviously, I_{m1} and I_{m2} are the quadratic functions of I_{in}. As cascading the simple quadratic circuits, we can obtain a higher order polynomial function which should be used to generate different curvatures by controlling the bending factors. In Fig. 4, we create a pseudo S-shape correction curve to illustrate the characteristic of the correction S-shape. In addition, we may take some operations such as bending, rotation, condensation, and shifting on the curves in Fig. 4 to realize an S-shape correction. The proposed circuits were simulated by using the 0.35 μm TSMC CMOS process and HSPICE. The supply voltage is set to be 3.3 V. The input current is from 0 μA to 220 μA.

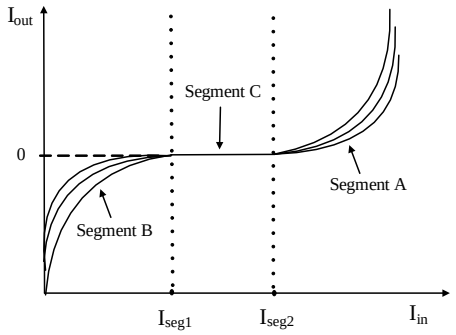

Fig. 4 Three segmented curve with different curvatures.

3.1 Curve Bending Circuit

Figure 5 shows the curve generator of Segment A which sketched in Fig. 4. When I_{in} is small, I_{ma} is large from Eq. (1). Because $I_{ma} + I_a = I_{r2} - I_{r1}$, I_{r1} will be small for small I_{in}. As $I_{ma} + I_a$ is large enough, Ma1 is forced to operate in cutoff. Therefore, we can use the bias current I_a to control the cutoff point. When I_{in} is large enough, I_{ma} will be small from Eq. (1), Ma1 will be on. If I_{in} increases, then I_{r1} and I_{sa} will increase. Figure 6 shows the simulation results of I_{sa}. As we tune the width of Ma3, we can change the curvature of Segment A. Therefore, Fig. 5 shows the curve bending circuit of Segment A. The size of Ma3 is the curve bending factor.

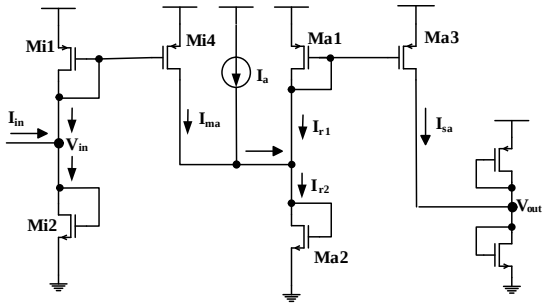

Fig. 5 Curve bending circuit of Segment A.

Figure 7 shows the curve generator of Segment B which sketched in Fig. 4. When I_{in} is small, we find the I_{mb} is large. Because $I_{mb} - I_b = I_{f2} - I_{f1}$, I_{f2} will be large, the large amount of $I_{mb} - I_b$ will drive Mb2 operating in saturation. When I_{in} increases, I_{mb} will decrease, I_{f2} and I_{sb} will decrease. If I_{in} is large enough, then Mb2 will operate in cutoff. Figure 8 shows the simulation results of $-I_{sb}$. Therefore, when we tune the width of Mb3, we can change the curvature of Segment B. Consequently, Fig. 7 shows the curve bending circuit of Segment B. The size of Mb3 is the curve bending factor.

3.2 Curve Rotating Circuit

Figure 9 shows the linear circuit. It is a simple current-

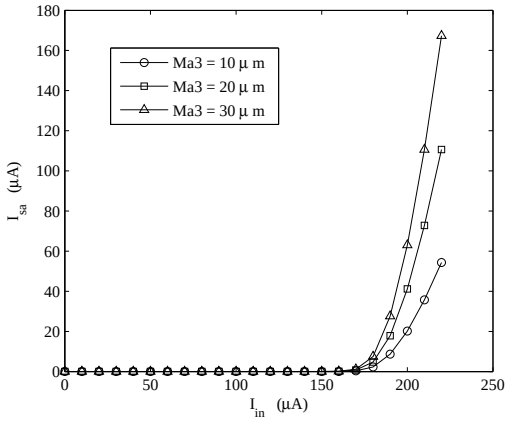

Fig. 6 Different curvatures for different widths of Ma3 at Segment A.

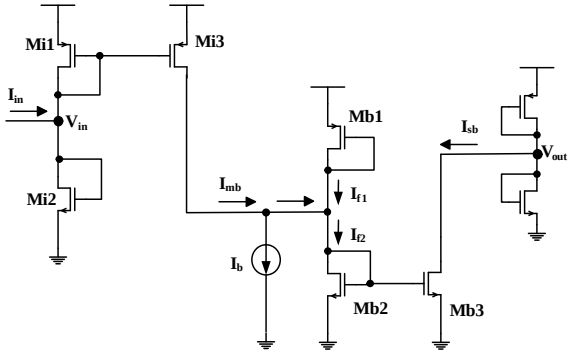

Fig. 7 Curve bending circuit of Segment B.

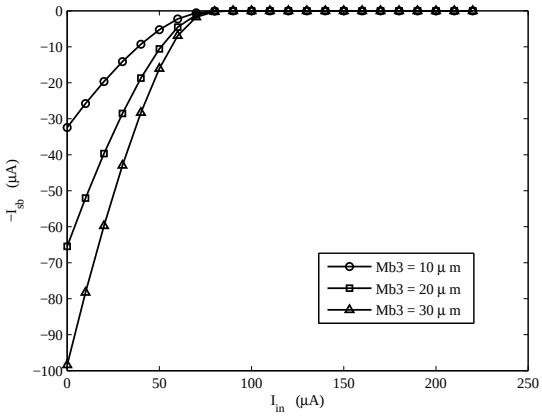

Fig. 8 Different curvatures for different widths of Mb3 at Segment B.

mirror. When the outputs of curve bending circuits are combined with the current-mirror, the curves in Fig. 6 and Fig. 8 are rotated. The linear characteristics and their rotating results are shown in Fig. 10 and Fig. 11, respectively. Figure 12 is the combined circuit of the bending circuit and the rotating circuit, where $I_{out} = I_{sa} - I_{sb} + I_{sc} + I_{dc}$. The current source I_{dc} is used in DC level bias. Different size of Mc2 represents different rotation angle. The size of Mc2 is the rotating factor.

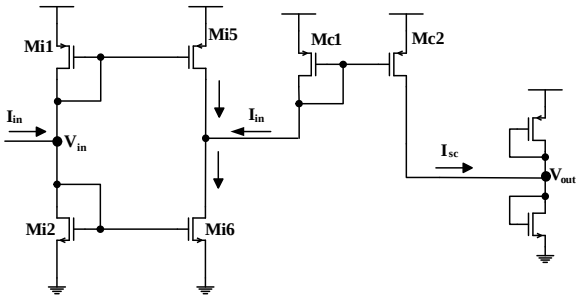

Fig. 9 Curve rotating circuit constructed by simple current-mirrors.

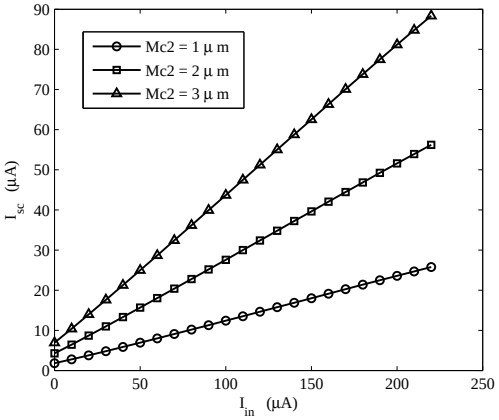

Fig. 10 The linear characteristics of curve rotating circuit.

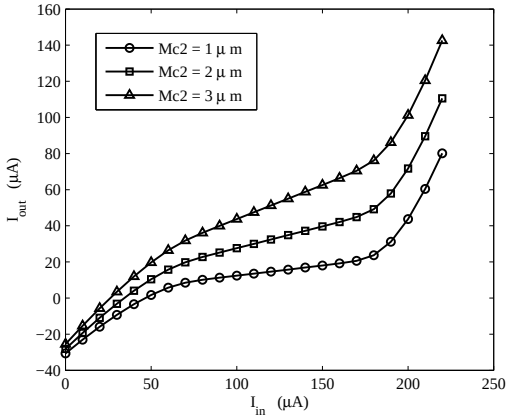

Fig. 11 Rotation results including Segment A and Segment B for different widths of Mc3.

3.3 Curve Condensing Circuit

When we tune the width of Mi3 and Mi4 in Fig. 12, we

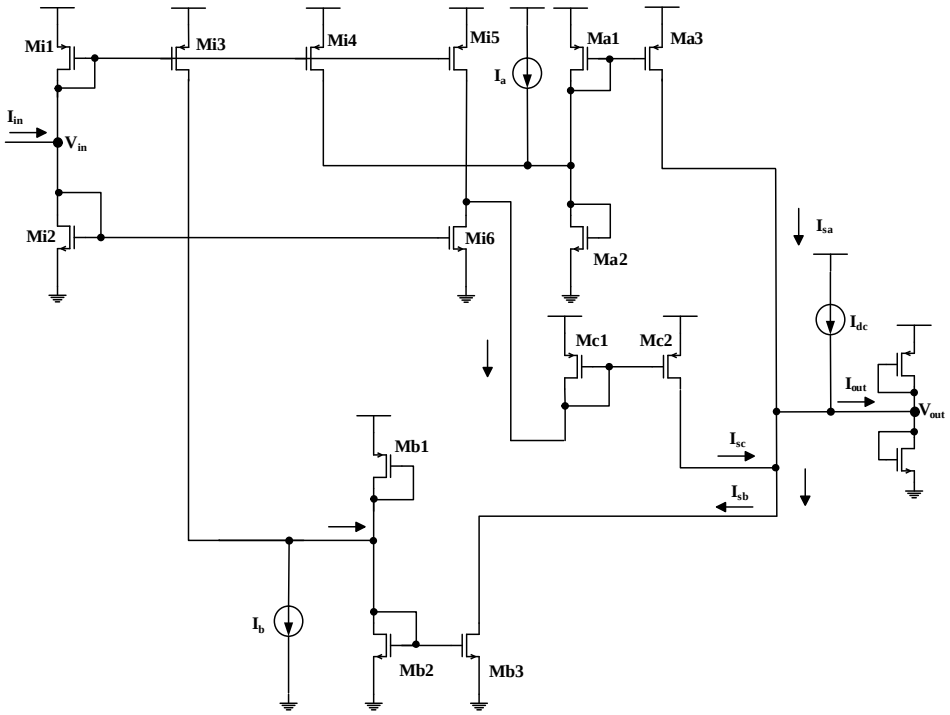

Fig. 12 A specified S-shape correction circuit.

could condense or expand the Segment C. Figure 13 shows the curve condensing results. The size of Mi3 and Mi4 is the condensing factor.

3.4 Level Shifting Circuit

In the current-mode circuit, we can easily make a level shift circuit by adding a constant current source I_{dc} at the output port shown in Fig. 12. Figure 14 shows the simulation results of level shift.

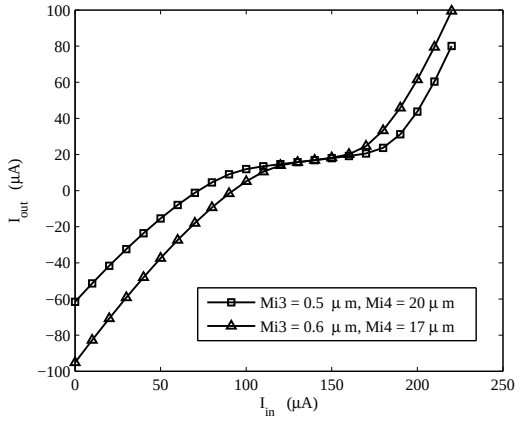

Fig. 13 Curve condensing results for different widths of Mi3 and Mi4.

3.5 Adjustable S-Shape Correction Circuit

Finally, we design an adjustable S-shape correction circuit

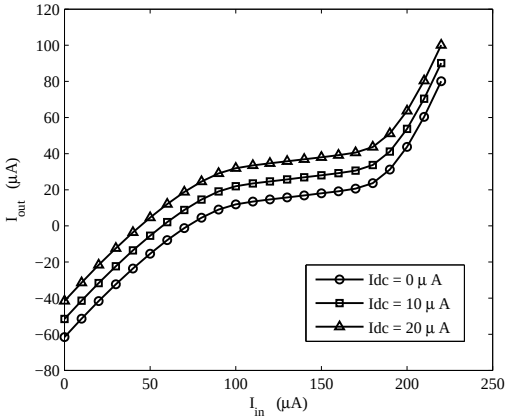

Fig. 14 Level shifting results for different value of I_{dc}.

shown in Fig. 15. We can tune a correction shape by giving a proper VDD or GND at the control points which are named with Cx for x from 1 to n.

4. Experimental Results

We trim the circuit in Fig. 15 into the circuit shown in Fig. 16 for fabricating. In Fig. 16, C1 is used for condensing the Segment C shown in Fig. 4 when C1 connects to VDD. C2 is designed to bend up the curve of Segment A when C2 connects to VDD. C3 and C4 are used to rotate the S-shape counterclockwise when C3 and/or C4 connect to VDD. As C5 connects to GND, the curve of Segment B will bend down. As C6 connects to GND, we can shift down the out-

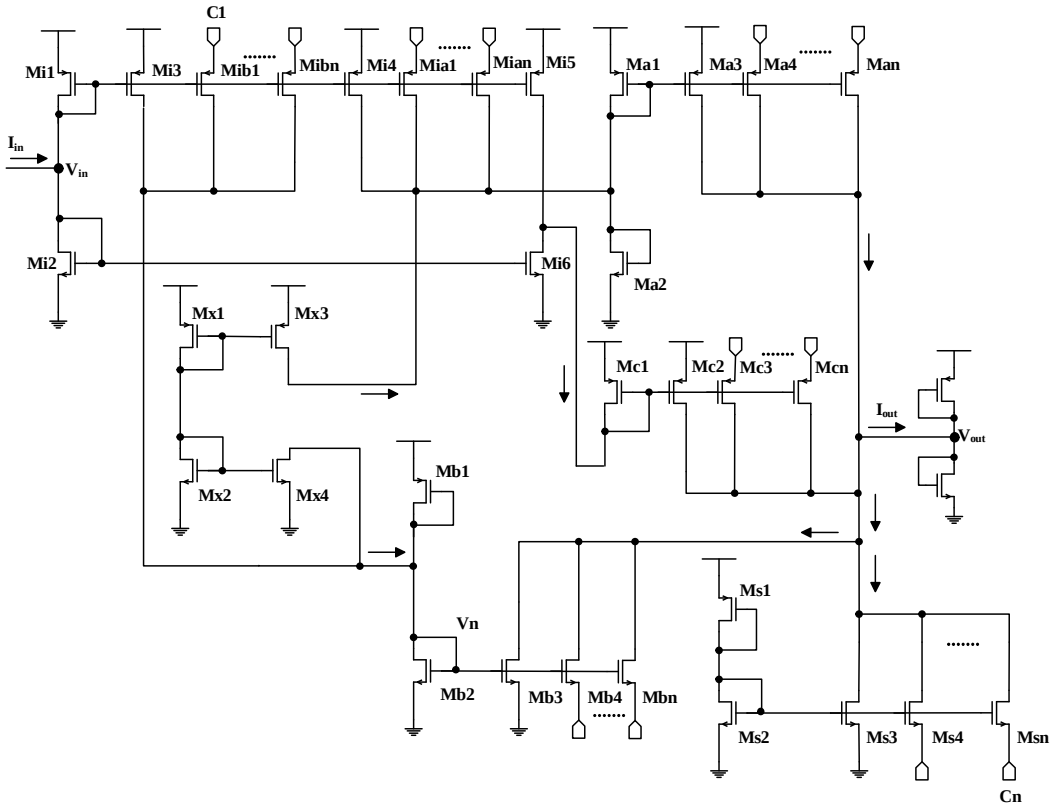

Fig. 15 An adjustable S-shape correction circuit with control points $C1, C2, \cdots, Cn$

put current level. The adjustable S-shape correction circuit was fabricated by using the $0.35\mu m$ TSMC CMOS process. The die photograph is shown in Fig. 17. The supply voltage (VDD) is 3.3 V. Since the available instruments for the measurement are in a voltage-mode, we use HSPICE to measure the input voltage (V_{in}) for every input current in the design stage. Then the input voltage can be applied to the inputs of the fabricated chip. We measure and record the V_{out} for the chip. Then we can obtain the I_{out} by comparing the V_{out} in the HSPICE. Figure 18 shows the measured results. In the experiment, we set the combination of (C1, C2, C3, C4, C5, C6) = (0, 1, 0, 1, 0, 0) as $s1$, and the combination of (1, 0, 1, 0, 1, 1) as $s2$, where 1 and 0 represent VDD and GND, respectively. We observe $s1$ is more condensed then $s2$, and $s2$ is less bended than $s1$, which prove the control functions of (C1, C2, C3, C4, C5, C6). Therefore, if we add more control points, we can flexibly match different S-shape from different manufactures by using bending, shifting, rotating, and condensing. Furthermore, we could overcome the errors due to process variations by adjusting some control points. For conventional methods like [3]–[6], which use variable resistors to adjust the S-shape considering the functions of bending, shifting, and rotating but not including the condensing function. Moreover, the mass resistors in conventional methods increase the chip size. The conventional methods use DACs to express the electro-optical transfer functions [3]–[6], which are not related to the input

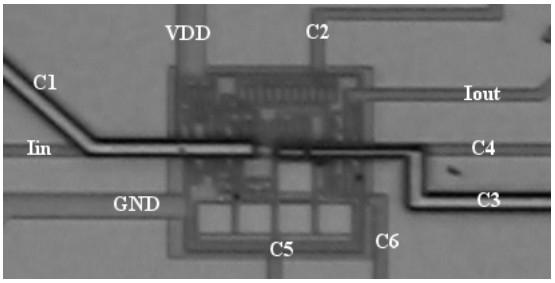

Fig. 17 Die photograph.

dynamic range. The resolution of DAC represents the curve resolution of S-shape correction. In analog circuit design, however, it is important for S-shape correction with large input dynamic range which will increase the tuning resolution of S-shape correction curve. It is observed in Fig. 18, the input dynamic range of I_{in} is from 0 μA to 220 μA, which is large in analog electro-optical transfer function for comparing to the voltage-mode range from 1.35 V to 1.75 V in [7].

For observing the frequency responses, we add a small signal $20 sin 2\pi f_0 t$ (denoted by I_{sin} with an unit of μA) to the input of I_{in}. By changing f_0 from 1 KHz to 300 MHz, we could measure and record the AC output denoted by I_{fout}. As the amplitudes of I_{fout} and I_{sin} are denoted by A_{fout} and A_{sin}, respectively, we can calculate each transfer function of $20\log(\frac{A_{fout}}{A_{sin}})$. If the maximum value of $20\log(\frac{A_{fout}}{A_{sin}})$ is set to

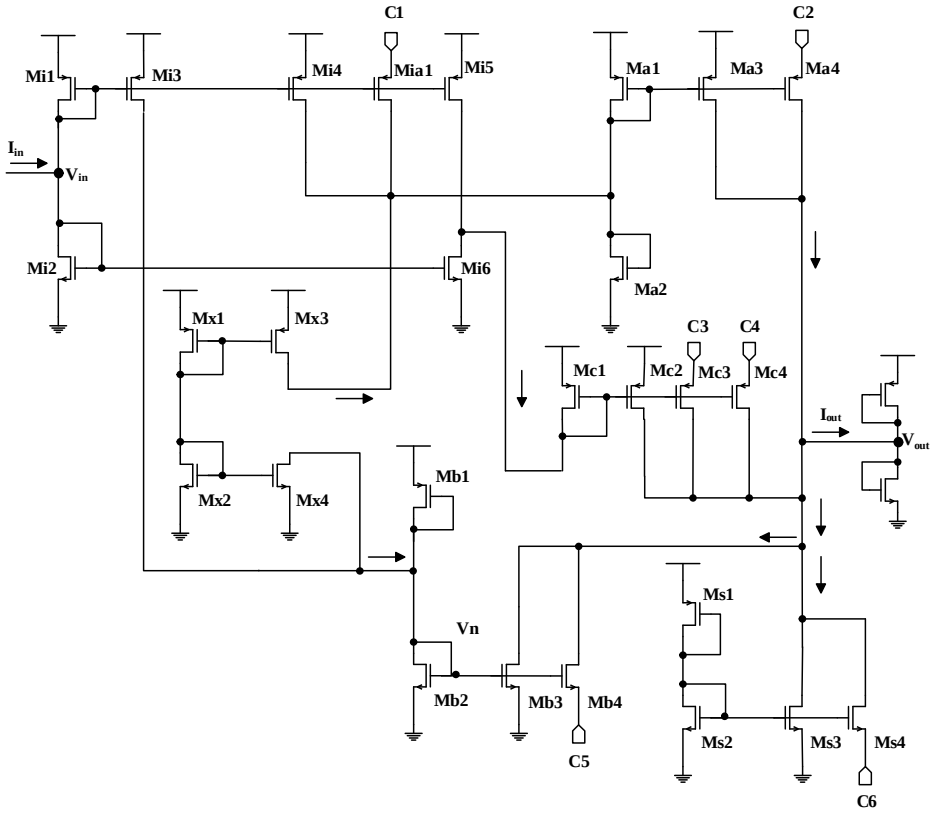

Fig. 16 A trimmed adjustable S-shape correction circuit for fabrication.

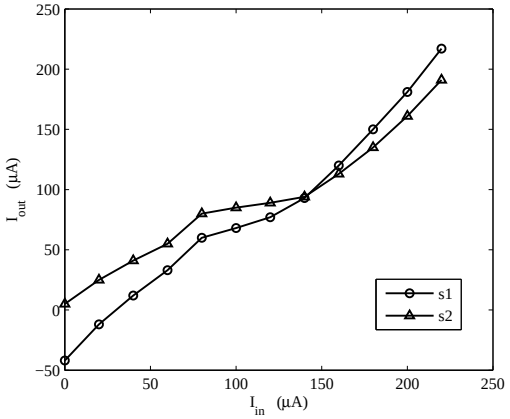

Fig. 18 The measured results of the S-shape correction circuit. The shape $s1$ is the combination of (C1, C2, C3, C4, C5, C6) = (1, 0, 1, 0, 1, 1). The shape $s2$ is the combination of (C1, C2, C3, C4, C5, C6) = (0, 1, 0, 1, 0, 0).

be 0 dB, then the bandwidth measurements are plotted in Fig. 19, where the locations of -3 dB are at 97 MHz, 190 MHz, and 262 MHz for I_{in} being 25 μA, 100 μA, and 175 μA, respectively. We observe that the -3 dB bandwidth is related to the value of I_{in}. Even though a lower value of I_{in} will decrease the bandwidth, the frequency responses in lower current region are still good for -3 dB bandwidth near 100 MHz when comparing to [7] with -3dB bandwidth of 7 MHz and [12] with -3dB bandwidth of 0.8 MHz.

We utilize the measurement result of S-shape correction curve $s2$ shown in Fig. 18 and MATLAB programs to demo an image correction. We map the output current range from 5 μA to 195 μA to the grey levels from 0 to 255. Since each output current responses an input current, we can establish a correction array, which records the mapping grey-levels for the input current. If the input current range from 0 μA to 220 μA is divided into 256 segments, then the correction array can be index by 256 grey levels instead of the input current. Consequently, a pixel grey level in the input image can indicate an output grey level through the correction array. Therefore, the image with an S-shape characteristic shown in Fig. 20(a) will be corrected to the image shown in Fig. 20(b) by performing the mapping process. The corrected image obviously compress the pixel intensity value of the bright image to a darkness part from the observation of the image histogram, which are generated by MATLAB functions.

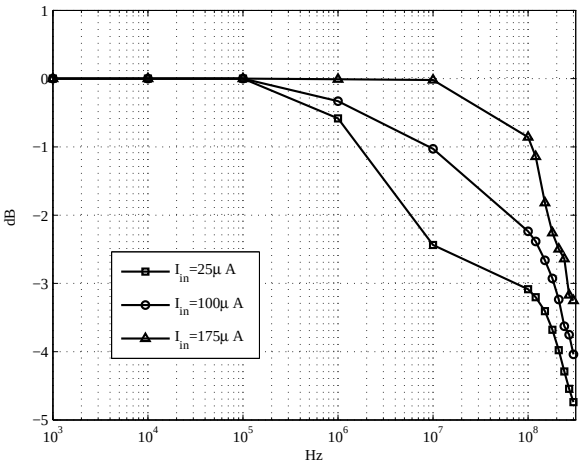

Fig. 19 Bandwidth measurement results for I_{in} being 25 μA, 100 μA, and 175 μA.

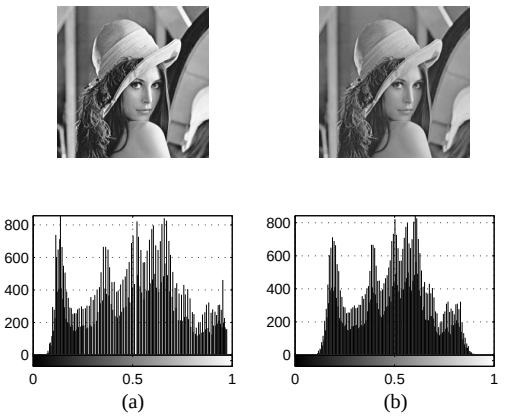

Fig. 20 The measured results of S-shape correction. (a) uncorrected image and its histogram. (b) S-shape corrected image and its histogram.

5. Conclusion

In this paper, we have proposed a novel S-shape correction curve generator based on a CMOS current-mode circuit. In particular, due to different S-shape LCD manufactures, one can adjust the shape form by switching the values of control points. The circuit design and simulation results have been presented step by step. We can observe that the shape form generation is very flexible. Furthermore, we have measured the test data and presented its performance from the fabricated chip. In the future, we could expect the reliability of generating a shape by setting more control points for compensating process variations.

Acknowledgments

The authors would like to thank the National Chip Implementation Center (CIC) of the National Applied Research Laboratories of Taiwan for chip fabrication. The research is supported by the National Science Council of Taiwan, under Grant No. NSC100-2221-E-216-033.

References

[1] Sony Corporation, Colour Matching Technology: BVM-L Series LCD Master Monitor, Sony Corporation, 2009.
[2] A. Molnár and K. Samu, The Examinations of the LCD Monitor Parameters in Case of the RGB Basic Colour-Stimuli, XI International PhD Workshop, pp. 190-192, 2009.
[3] P. M. Lee and H. Y. Chen, Adjustable Gamma Correction Circuit for TFT LCD, IEEE International Symposium on Circuits and Systems, vol. 1, pp. 780-783, 2005.
[4] M. Olivieri, R. Mancuso, and F. Riedel, A Reconfigurable, Low Power, Temperature Compensated IC for 8-Segment Gamma Correction Curve in TFT, OLED and PDP Displays, IEEE Transactions on Consumer Electronics, vol. 53, no. 2, pp. 720-724, 2007.
[5] C. W. Park and J. Y. Ryu, Development of a New Automatic Gamma Control System for Mobile LCD Applications, Displays, vol. 29, pp. 393-400, 2008.
[6] D. J. R. Cristaldi, S. Pennisi, and F. Pulvirenti, Liquid Crystal Display Drivers: Techniques and Circuits, Springer, 2009.
[7] Y. Li, C. Wang, X. Lai, and X. Li, Nonlinear Compensating Circuit for LCD Driver, 5th International Conference on ASIC, vol. 1, pp. 631-634, 2003.
[8] Y. Kwak and L. MacDonald, Characterisation of a Desktop LCD Projector, Displays, vol. 21, issue 5, pp. 179-194, 2000.
[9] T. Florin and N. E. Mastorakis, An Overview about Monitors Colors Rendering, WSEAS Transactions on Circuits and systems, vol. 9, issue 1, pp.32-41, 2010.
[10] K. J. Lin, C. J. Cheng, S. F. Chiu, and J. E Chen, CMOS Current-Mode Selectable S-Shape Correction Circuit, Proceedings of the 9th WSEAS Int. Conference on Instrumentation, Measurement, Circuits and Systems, China, pp. 70-75, 2010.
[11] A. Motamed, C. Hwang, and M. Ismail, CMOS Exponential Current-to-Voltage Converter, Electron. Lett., vol. 33, no. 12, pp. 998-1000, 1997.
[12] Texas Instruments, Multi-Channel LCD Gamma Correction Buffer-Check for Samples: BUF07703, BUF06703, BUF05703, SBOS269CMARCH-2003REVISED, April 2010.

Kuo-Jen Lin was born in Ilan, Taiwan, in 1963. He received the B.S. degree in electronics engineering from Tamkang University, Taipei, Taiwan, in 1985 and the M.S. degree in electrical engineering from Chung Hua University, Hsingchu, Taiwan, in 1997. In 2004, he obtained the Ph.D. degree in Computer Science and Information Engineering from National Central University, Taoyuan, Taiwan. From 1997 to 2004, he was an Assistant Researcher at Chung Shan Institute of Science and Technology, Taiwan. He is currently an Associate Professor in the Department of Electronics Engineering, Chung Hua University, Hsingchu, Taiwan. His research interests are CMOS current-mode circuit design, synthesis for current-mode circuit, and design in direct digital frequency synthesizers. Dr. Lin is a member of the Institute of Electronics, Information and Communication Engineers.

Chih-Jen Cheng was born in Hsinchu, Taiwan, in 1984. He received the B.S. and M.S. degrees from Chung Hua University in 2007 and 2009,respectively. He is currently working toward the Ph.D. degree at National Central University of Electrical Engineering. His research interests include VLSI circuits design, and analog signal processing.

Hsin-Cheng Su was born in Taipei, Taiwan, in 1986. He received the B.S. degree from Tamkang University in 2008 and M.S. degree from Chung Hua University in 2011. His research interests include CMOS current-mode circuit design and image processing.

Jwu-E Chen received the B.S., M.S., and Ph.D. degrees in electronic engineering from National Chiao-Tung University, Hsinchu, Taiwan, R.O.C., in 1984, 1986, and 1990, respectively. Presently, he is an Associate Professor in the Department of Electrical Engineering, National Central University, Chung-li, Taiwan, R.O.C. His research interests include multiple-valued logic, VLSI testing, synthesis for testability, reliable computing, yield analysis, and test management. Dr. Chen is a member of the IEEE Computer Society.

附件四

國科會補助專題研究計畫出席國際學術會議心得報告

日期：101 年 8 月 15 日

計畫編號	NSC 100－2221－E－216－033－		
計畫名稱	使用多段曲線擬合方法實現 CMOS 電流模式函數		
出國人員姓名	鄭智仁	服務機構及職稱	中央大學電機所博士班
會議時間	101 年 7 月 27 日至 101 年 7 月 29 日	會議地點	中國瀋陽
會議名稱	(中文)電子學與光電子學國際會議(ICEOE 2012) (英文)International Conference on Electronics and Optoelectronics		
發表題目	(中文)利用多段近似法之電流模式雙曲正切 Sigmoid 函數 (英文)CMOS Current-Mode Hyperbolic Tangent Sigmoid Function Implementation Using Multi-Segment Approximation.		

一、參加會議經過

電子學與光電子學國際會議（International Conference on Electronics and Optoelectronics）為舉辦一次的國際學術研討會，今年為第二屆於 2012 年 7 月 27 日至 7 月 30 日在中國瀋陽舉行，會議開始第一天 (7/27)，午後 2 點進入會場前往註冊；註冊時間至當天下午的 5 點。

會議的第二天(7/28))主要的議程為分為上午 OEMR 2012 與下午 ICEOE 2012 會議。在 OEMR 會議討論 CCD、EMCCD 與 PLC 等議題，下午為 ICEOE 會議討論此次所發表利用多段近似法之電流模式雙曲正切 Sigmoid 函數，每場演講後的討論正是各個學者意見互相交流的時間，可以相互激發思慮，讓我受益良多。晚間餐參與大會舉辦的歡迎晚餐，並感謝會議人員的盛情招待。

二、與會心得

首先感謝國科會計畫對於這次國際會議研究計畫的經費補助和支持，除了吸收世界各地優秀學者所提供的研究資訊之外，對於這種直接面對面交流與觀摩的機會，與會者提出的最新成果和交流思想對提升新技術的研究開發和應用微波材料都能促進更多技術的提升也更能夠提升國內的研究水準，並提高台灣在國際學術研究上的能見度。

三、發表論文全文或摘要

We propose a multi-segment approximation method to design a CMOS current-mode hyperbolic tangent sigmoid function with high accuracy and wide input dynamic range. The dynamic range is dependent on the number of segments and the accuracy is related to the dividing point. From mathematical results, we can observe the proposed method outperforms traditional methods. We implement the multi-segment approximation circuit to realize the hyperbolic tangent sigmoid function. The simulation results of the proposed circuit show a wide input dynamic range from -256μA to 240μA for relative error less than 3% and a high bandwidth of 138 *MHz*.

四、建議

參加國際學術研討會，對於學術上是很好的學習，可與不同國家學者相互討論，希望往後能有更多機會與管道與幫助學生多參加國際研討會。

五、攜回資料名稱及內容

1. Program and Book of Abstracts:內容為會議議程投稿者之論文摘要。
2. 大會附贈環保袋一只

六、其他

無。

ICEOE2012 and OEMR2012 CONFERENCES SCHEDULE

2012 2nd International Conference on Electronics and Optoelectronics (ICEOE 2012)

2012 International Meeting on Opto-Electronics Engineering and Materials Research (OEMR 2012)

Tianlun Regar Hotel Shenyang

Shenyang, China

July 27 - 28, 2012

July 27, 2012 (Friday)

Lobby of Tianlun Regar Hotel Shenyang (沈阳天伦瑞格酒店大厅)

10：00 – 12：00 14：30 – 18：00	Arrival and Registration

Note：(1) You can also register at any time during the conference.

(2) Certificate of Participation can be collected at the registration counter.

(3) The organizer won't provide accommodation, and we suggest you make an early reservation.

Morning, July 28, 2012 (Saturday)

RUIHE A Hall of The Sixth Floor

6 层瑞和 A 厅

Time: 9:00-12:00

OE0150	Characteristic of Point Defect around the Photonic Crystal Bend
	Ruei-Chang Lu, Chun-Min Wang and Keh-Yi Lee
OE0151	Wavelength Division Multiplexer based on Periodic Dielectric Waveguide Ring Resonator
	Ruei-Chang Lu, Tung-Hao Chen and Yu-Ping Lia
OE0800	A new design of large area MCP-PMT for the next generation neutrino experiments
	Sen. Qian
OE0183	Noise Analysis of EMCCD and Optimum Design of Its Operating Mode
	Yugui Zhang,Tao Li and Zhikuan He
OE0590	Optimal Design of CCD Driving Signal Based on FLEX 10K
	Zhikuan He, Songbo Wu and Yugui Zhang
OE0239	A 5-port Photonic Lantern for Light Beam Combining
	Yan Qi, Haijiao Yu,Fengjun Tian and Weimin Sun
OE0539	CPU Experiment of Heat Dissipation and Temperature Rise
	Maode Li,Wei Wei and Yi Li
OE0235	Influence of Pump Light's Duty Cycle on Cesium Atomic Magnetometer
	Xianjin Zeng, Junhai Zhang, Qiang Liu, Zongjun Huang and Weimin Sun
OE0645	Influence of Plasmonic Light-Scattering by Gold Nano-island Structures on the Quantum Efficiency of Organic Solar Cell
	Baozeng Wang,Xinping Zhang and Jian Zhang
OE0646	Directly-Written Metallic Photonic Crystals for Sensor Applications
	Jian Zhang,Xinping Zhang,Zhaoguang Pang and Baozeng Wang
OE0195	The Effects of Pump Beam on Cesium Magnetometer Sensitivity
	Qingmeng Li, Qiang Liu, Junhai Zhang, Zongjun Huang, Xianjin Zeng and Weimin Sun
OE0584	Measurement of SO2 using Differential Optical Absorption Spectroscopy
	Haiming Zheng, Zhenliang Dong, Dongshui Xie and Xiaoxiao Shang

OE0109	Study On Control Technology of Double-fed Motor Based On PLC and General Invert
	Chengwu Lin, Jialin Shi and Bo Lu
OE0110	Research on Grid-connected Inverter Based on Current Track Control in Wind Generation System
	Chengwu Lin, Qiguang Jiang and Li Ma
OE0568	A new Coupled PDE Method for Image Processing
	Maolin Wang, Jun Yue, Pan Huang and Chaoshuai Song
OE0214	Comparison of Gold and Silver Nanoparticles as Active Substrates for SERS Spectra Measurements on Liver Cancer Cells
	Chen Qian,Shupeng Liu,Na Chen,Zhenyi Chen and Qianqian Geng
OE0202	Generation of Multi-Atom W States in Microtoroidal Cavity-Atom System
	Yu Huang
OE0165	A Method for Lidar Data Conversion and Standardization
	Hao Chen, Dengxin Hua, Yikun Zhang, Zhirong Zhou, Shichun Li and Li Wang
OE0233	The structural design of combined absorber composed by MPP and multi-layer porous material based on VA One
	Xiuhua Duan, Huanqin Wang,Wenjuan Sun and Deyi Kong
OE0537	Studying Relative Error Formulae of Surveying Textbooks of Chinese Colleges
	Yonghe Deng
OE0245	Dynamically manipulating beam with metallic nano-optic lens containing liquid crystal
	Jicheng Wang, Xia Zhou,Jie Gao,Zhetao Xu, Lin Sun and Xiao Jin
OE0550	Solvothermal method preparation of nano Y2O2SEu3+ and research of luminescence property
	Lu Lu and Zhilong Wang

12：00 - 13：30	Lunch Break

Afternoon, July 28, 2012 (Saturday)

RUIHE A Hall of The Sixth Floor

6 层瑞和 A 厅

Time: 14:00-18:00

CE0105	Fault diagnosis of COIL based on BP Artificial Neural Network
	Zheng Zhang, Shiqiang Zhang, Yanhong Sun
CE0121	Study of Top Triangular Nano-grating on Solar Cell Using Rigorous Coupled Wave Analysisg
	Xiaomin Jin, Douglas Alan Cattarusa, and Michael James Marshall
CE0126	Comparative Research on Different Solutions of a High-Performance Thin-Film Polarizing Beam Splitter
	Kaiyong Yang, Hongchang Zhao, Yunfeng Jia, Suyong Wu
CE0140	Optimization Of Fiber Length For Edfa To Enhance The Channel Capacity Of Dwdm System
	Inderpreet Kaur, Neena Gupta
CE0143	Long-haul Wavelength Division Multiplexing Secure Communications with Chaotic Optical Channels
	Xiaolei Chen, Qingchun Zhao, Hongxi Yin, Xinyu Dou
CE0145	Optical-Mode Study of Galium Nitrate Based Laser Diodes
	Douglas Alan Cattarusa, Xiaomin Jin, Xiao-Hua Yu, Xing-Xing Fu, Xiang-Ning Kang, Bei Zhang, Guo-Yi Zhang
CE0157	A simple mechanism to suppress the mode competition for stable and tunable dual-wavelength erbium-doped fiber lasers
	Chenfang Zhang, Jiang Sun, Siwen Zheng and Shuisheng Jian
CE0166	Application of Optical Phase conjugation in Adaptive optics to remove atmospheric aberrations from an optical wavefront
	Sriram Rengarajan, Nandhakishore Perarulalan
CE0172	Study on Optical Performance Monitoring for Fiber-optical Link Utilizing Chaos Theory
	Qingqing Fan, He Li, Hongxi Yin
CE0186	Multi-Point Correction Method in CMOS Current-Mode Function Design
	Kuo-Jen Lin, Chih-Jen Cheng, Jwu-E Chen
CE0199	CMOS Current-Mode Hyperbolic Tangent Sigmoid Function Implementation Using Multi-Segment Approximations
	Chih-Jen Cheng, Kuo-Jen Lin, Jwu-E Chen
CE0235	The development of Remote Measurement System Based on GSM Internet of Things(IOT)
	Yunxin Gong, Houyu Zhao
CE0245	Research of Temperature Compensation for Ultrasonic Rangefinder
	Gang Tian, Jun Gui
CE0247	Analysis on the Relationship Between Burst Errors and Tracking Control Frequency in Satellite-to-Ground Laser communications
	Qiwen Ran, Zhonghua Yang, Jing Ma, Liying Tan, Shichen Wu, Qingfeng liu, Huixi

	Liao
CE0273	The three-dimensional analysis of light scattering characters for Rayleigh particles on/below the wafer
	Lei Gong, Zhensen Wu
CE0282	Simulation of Laser Beam Scattering from Complex Targets in the Near Field
	Jiaxuan Lin, Zhensen Wu, Xiang Su, Biao Wang
CE0284	The Analysis of Influencing Factors of One Dimensional Range Profiles and Surface Elements Imaging Method to Arbitrary Target
	Yuan Mou, Zhensen Wu, Zhuo Chen, Hanlu Zhang
CE0285	Scattering Properties of the Higher-Order Hermite Gaussian Beam
	Tan Qu, Zhensen Wu, Haiying Li, Zhengjun Li
CE0287	Extraordinary Electromagnetic Scattering of Plane Wave by Double Negative Coated Sphere
	Yan'e Shi, Zhensen Wu, Hongfei Tian, Zhengjun Li
CE0288	Scattering Characteristics of Complex Target from Solar Irradiance and Sky-ground Background Radiance in Infrared Spectrum
	Xing Guo, Zhensen Wu, Longxiang Linghu, Yufeng Yang
CE0289	Scattering of Two-Dimensional Sea Surface at Low Grazing Angles with Physical Optics Method
	Zhuo Chen, Zhensen Wu, Yong Zhang, Jingjing Xue, Wenhua Ye
CE0292	The Acceleration of PO Based on CUDA
	Xiang Su, Zhensen Wu, Jiaxuan Lin and Xiaobing Wang
CE0293	Decomposing the Non-Gaussian Surface in Sum of Gaussian Surfaces
	Zhangxing Qi, Zhensen Wu, Ziwen Yu, Haiying Li
CE0294	Polarization Properties of Scattered Fields from a Chiral Sphere
	Qingchao Shang, Zhensen Wu, Peng Zhao, Zhengjun Li
CE0311	Phase-only Beam Optimization for GaAs Optical Waveguide Phase Array
	Yong Zhang
CE0314	Path loss of Non-Line-of-Sight single-scatter model
	Tairong Wang, Lu Bai, Zhensen Wu
CE0316	Adaptive Interleaving Method and its Application to Free Space Optical Communications through Atmospheric Turbulence Channel
	Zhonghua Yang, Qiwen Ran, Jing Ma, Liying Tan, Shichen Wu, Qingfeng liu, Huixi Liao

18：00 - 19：30	**Buffet Dinner**

CMOS Current-Mode Hyperbolic Tangent Sigmoid Function Implementation Using Multi-Segment Approximations

Chih-Jen Cheng
Department of Electrical Engineering
National Central University
Taoyuan, Taiwan
Email: 985401005@cc.ncu.edu.tw

Kuo-Jen Lin (corresponding author)
Department of Electronics Engineering
Chung Hua University
Hsinchu, Taiwan
Email: kuojenlin@chu.edu.tw

Jwu-E Chen
Department of Electrical Engineering
National Central University
Taoyuan, Taiwan
Email: jechen@ee.ncu.edu.tw

***Abstract*—We propose a multi-segment approximation method to design a CMOS current-mode hyperbolic tangent sigmoid function with high accuracy and wide input dynamic range. The dynamic range is dependent on the number of segments and the accuracy is related to the dividing point. From mathematical results, we can observe the proposed method outperforms traditional methods. We implement the multi-segment approximation circuit to realize the hyperbolic tangent sigmoid function. The simulation results of the proposed circuit show a wide input dynamic range from $-256\mu A$ to $240\mu A$ for relative error less than 3% and a high bandwidth of 138 MHz.**

I. Introduction

In the era of increasingly sophisticated electronic technology, to handle complicated applications often must rely on more complicated functions to assist in the circuit design. The hyperbolic tangent sigmoid function (tanh), which is used as the transfer function of the artificial neural network (ANN) for the input layer and the hidden layer. In the previous literature, the tanh function is designed by using digital circuits [1], [2], which occupy a large area and high power consumption. In [3], authors implement the tanh function by using analog circuits, which are composed of CMOS circuits operated in weak inversion. However, the speed, input dynamic range, and accuracy for these applications are limited. For improving the speed and the total harmonic distortion (THD), Berg et al. proposed a floating gate CMOS to implement the tanh function [4]. CMOS current-mode circuit naturally becomes the most favorable circuit. Most of CMOS current-mode circuits operate in the saturation region for high speed applications [5]–[7]. In the region, the square law characteristic of a MOS can be applied to design different functions such as exponential circuits [6], [8], geometric-mean circuits [5], [7], and fuzzy logic circuit [7]. Several applications [6], [8], [9] also use the second-order Taylor's approximations to approach the functions. However, the input dynamic range of the second-order Taylor's approximations are also limited for accuracy requirement.

In this paper, we propose a multi-segment approximation circuit to realize a tanh function with the characteristics of high speed, wider input dynamic range, and high accuracy. We divide the function into four segments. Each segment, we use the quadratic polynomial approach to reduce the complexity of the circuit. The dividing point should be dependent on the required accuracy. The number of segments should relate to the input dynamic range.

II. Multi-Segment Approximation Method

The sigmoid function is non-linear, continuous, and differentiable, allowing it to map complex relations and provide a closed form when weights are updated during training of the neural network [10]. The tanh(x) could be approximated by Taylor's series for the expansion point at $x = 0$:

$$tanh(x) = x - \frac{x^3}{3} + \frac{2x^5}{15} - \frac{17x^7}{315} + \cdots \quad (1)$$

In Eq. (1), the x^3, x^5, and even x^7 are very difficult to implement by using CMOS current-mode circuits. Therefore, we divide the $tanh(x)$ into four segments which could be realized by second-order polynomials. We need to re-expand the $tanh(x)$ at different points a_i, the middle value of segment i, for using the Taylor's series:

$$tanh_i(x) \approx p_i x^2 + q_i x + r_i \quad (2)$$

where $p_i = -sech^2(a_i)tanh(a_i)$, $q_i = sech^2(a_i) - 2a_i p_i$, and $r_i = tanh(a_i) - a_i sech^2(a_i) + a_i^2 p_i$. When we select $a_1 = -1.68$, $a_2 = -0.56$, $a_3 = 0.56$, and $a_4 = 1.68$, we could approximate the $tanh_i(x)$ for different x intervals, respectively:

$$tanh_1(x) \approx 0.121x^2 + 0.537x - 0.373 \quad (x < -1.2) \quad (3)$$

$$tanh_2(x) \approx 0.377x^2 + 1.164x + 0.026 \quad (-1.2 \le x < 0) \quad (4)$$

$$tanh_3(x) \approx -0.377x^2 + 1.164x - 0.026 \quad (0 \le x < 1.2) \quad (5)$$

$$tanh_4(x) \approx -0.121x^2 + 0.537x + 0.373 \quad (x \ge 1.2) \quad (6)$$

Mathematical simulation results are shown in Fig. 1 for the four segmented approaches. For relative error less than 3%, the traditional Taylor's methods of expansion to the terms of x^3 , x^5, and x^7 have the input dynamic ranges of 1.3, 1.7, and

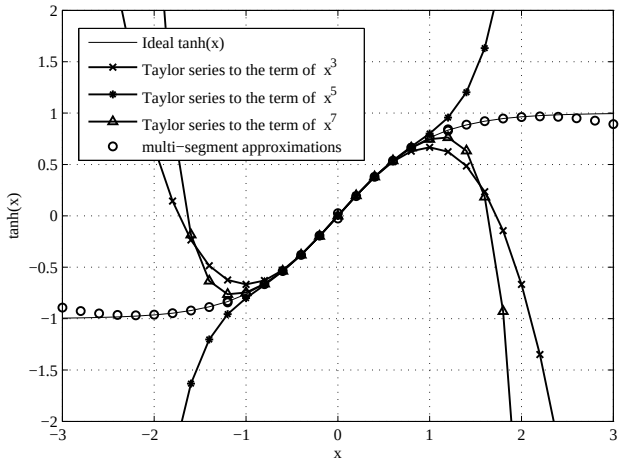

Fig. 1. Mathematical simulation results for different approximations.

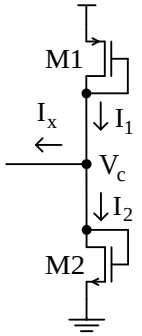

Fig. 2. Simple current-mode quadratic circuit.

2.0, respectively. The proposed multi-segment approximation reveals the wide input dynamic range of 5 for relative error less than 3%. Obviously, our proposed method outperforms the traditional methods.

III. Multi-Segment Approximation Circuit

The simulation result of Fig. 1 gives the good way to implement the tanh function by using four second-order polynomial functions. We will illustrate how to realize and control the four segments by using CMOS current-mode circuits.

A. Quadratic Circuit

We can generate a current-mode quadratic function by using a simple circuit shown in Fig. 2 [11]. From [12], we have two current-mode functions:

$$I_1 = K(\frac{V_{DD}-|V_{tp}|-V_{tn}}{2} + \frac{I_x}{2K(V_{DD}-|V_{tp}|-V_{tn})})^2 \quad (7)$$

$$I_2 = K(\frac{V_{DD}-|V_{tp}|-V_{tn}}{2} - \frac{I_x}{2K(V_{DD}-|V_{tp}|-V_{tn})})^2 \quad (8)$$

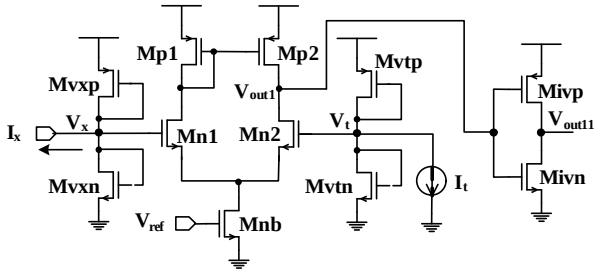

Fig. 3. Segment controller.

and

$$V_c = \frac{V_{DD}-|V_{tp}|+V_{tn}}{2} - \frac{I_x}{2K(V_{DD}-|V_{tp}|-V_{tn})} \quad (9)$$

Obviously, I_1 and I_2 are the quadratic functions of I_x. As I_x increases, V_c will decrease for observing Eq. (9). If we set $V_0 = \frac{V_{DD}-|V_{tp}|-V_{tn}}{2}$, then

$$I_1 = KV_0^2(1+\frac{I_x}{4KV_0^2})^2 \quad (10)$$

$$I_2 = KV_0^2(1-\frac{I_x}{4KV_0^2})^2 \quad (11)$$

If we set $I_0 = KV_0^2$ and $I_x = 4I_0x$. Equation (10) will be

$$I_1 = I_0(1+x)^2 \quad (12)$$

and (11) will be

$$I_2 = I_0(1-x)^2 \quad (13)$$

B. Segment Controller

We need to design a control circuit to switch the services of Eqs. (3), (4), (5), and (6). Therefore, we could design the segment controller shown in Fig. 3 based on a differential amplifier. If $I_x > I_t$, we have $V_x < V_t$, which make V_{out1} near ground (GND) and V_{out11} near VDD. Conversely, if $I_x < I_t$, we have the results of V_{out1} near VDD and V_{out11} near GND. For controlling four segments ($s1$, $s2$, $s3$, and $s4$), we need to construct a four-segments controller shown in Fig. 4. The V_{out1}, V_{out2}, and V_{out3} are controlled by I_{t1}, I_{t2}, and I_{t3}, respectively. A corresponding control table is shown in Table I.

In Fig. 4, the $s1$, $s2$, $s3$, and $s4$ segment circuits realize the Eqs. (3), (4), (5), and (6), respectively. The drain current of Mep12 is the scale of $I_0(1+x)^2$, we could size Mep12 and tune I_{b1} to make $I_0tanh_1(x)$ shown in Eq. (3). The $s2$ segment circuit also follows the sizing and tuning method. The $s3$ and $s4$ segment circuits will have $I_0tanh_3(x)$ and $I_0tanh_4(x)$. The $I_0tanh_3(x)$ is made by $AI_0(1+x)^2 - BI_0(1-x)^2$, where A and B are the scale of Mep32 and Men32, respectively, which are determined by Eq. (5) and tuned by observing the results of simulation. The similar work should apply on the generation of $I_0tanh_4(x)$.

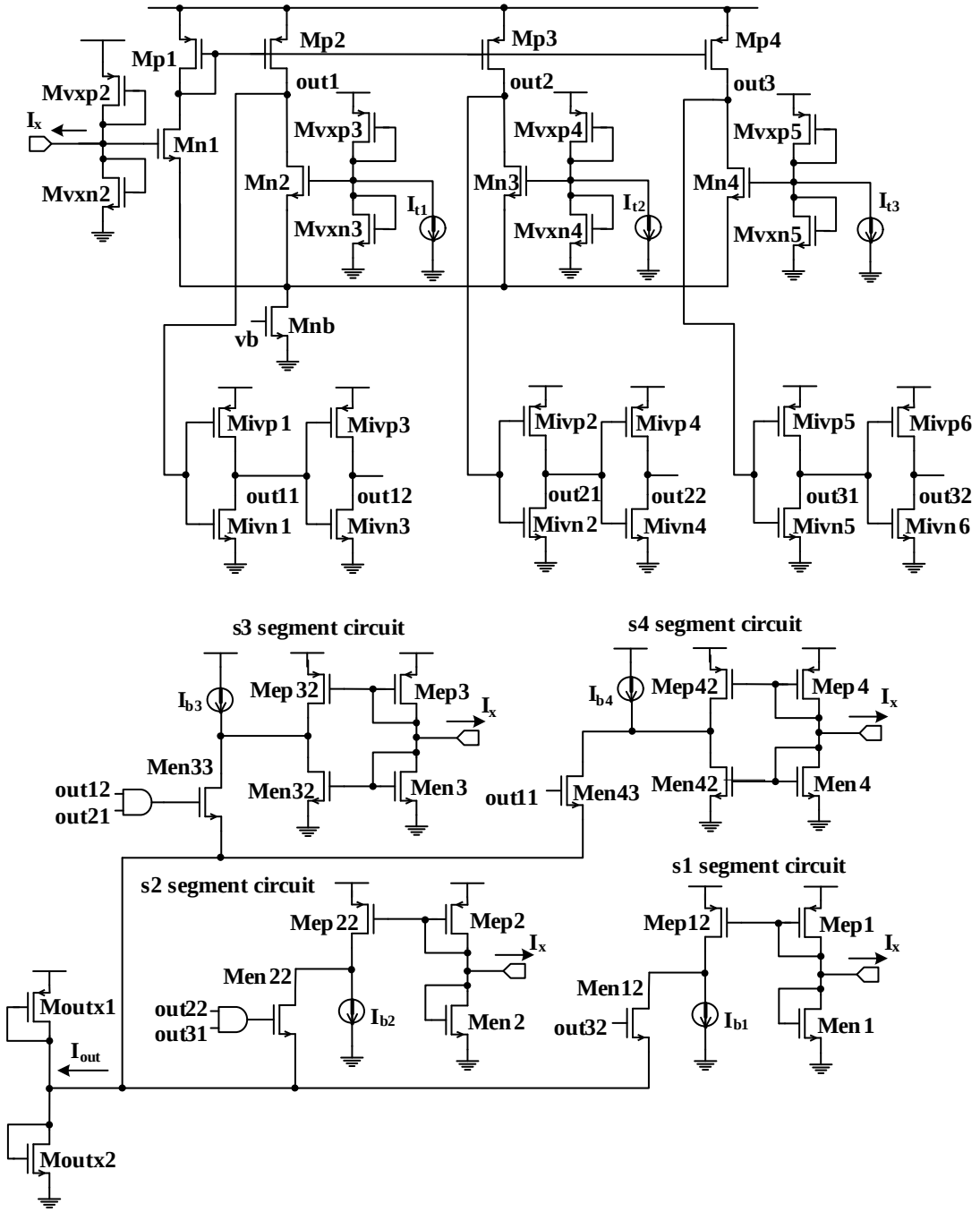

Fig. 4. Multi-segment approximation circuit for tanh.

IV. Simulation Results

To verify the multi-segment approximation circuit, we initiate a simulation by using the 0.35 μm CMOS TSMC technology. The supply voltage V_{DD} of the circuit in Fig. 4 is set to be $2.5V$. When we set $I_0 = 30\mu A$, we can observe I_x from $-300\mu A$ to $300\mu A$ for input dynamic range from $x = -2.5$ to $x = 2.5$. Figure 5 shows the I_{out} simulation results. The multi-segment approximation method nearly match the ideal tanh function for I_x from $-256\mu A$ to $240\mu A$ with relative error less than 3%. This range is mapped to x from -2.13 to 2.0. The total input dynamic range is about 4.13. The measured frequency response of I_{out} is shown in Fig. 6. The $-3dB$ bandwidth is 138 MHz. The THD measurements of I_{out} are shown in Fig. 7 for input DC current of $30\mu A$ and $130\mu A$ with sinusoidal signals of amplitude I_a from $2\mu A$ to $20\mu A$ at the frequency of 100 KHz.

V. Conclusion

In this paper, we propose a multi-segment method to design a CMOS current-mode hyperbolic tangent sigmoid function.

TABLE I
FOUR-SEGMENTS CONTROL TABLE.

Segment	s1 on $(I_x < I_{t3})$	s2 on $(I_{t3} \leq I_x < I_{t2})$	s3 on $(I_{t2} \leq I_x < I_{t1})$	s4 on $(I_x \geq I_{t1})$
V_{out11}	low	low	low	high
V_{out12}	high	high	high	low
V_{out21}	low	low	high	high
V_{out22}	high	high	low	low
V_{out31}	low	high	high	high
V_{out32}	high	low	low	low

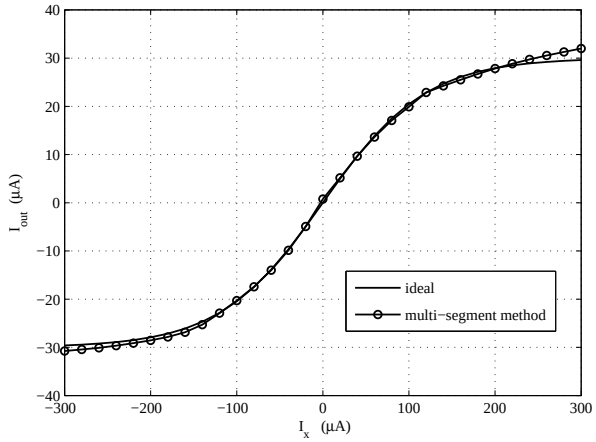

Fig. 5. Simulation results for current-mode tanh function.

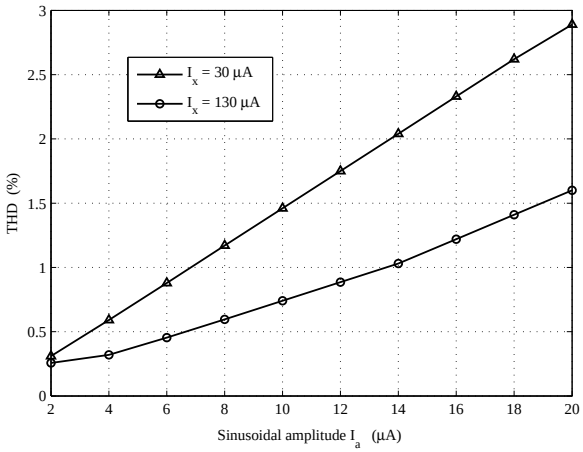

Fig. 7. THD measurement of the multi-segment approximation circuit.

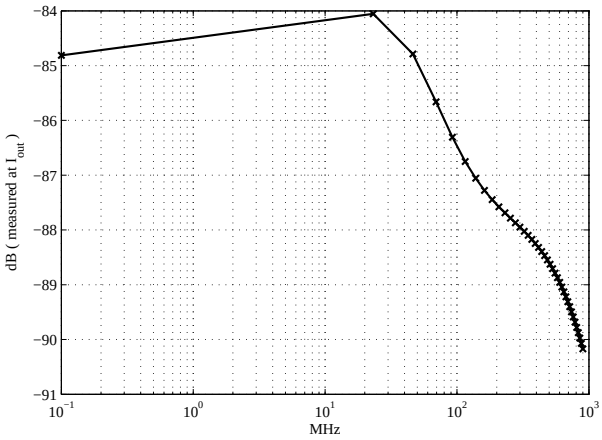

Fig. 6. Bandwidth measurement of the multi-segment approximation circuit.

The proposed multi-segment approximation circuit has been verified with wide input dynamic range from $-256\mu A$ to $240\mu A$ for relative error less than 3%, which is wider than the Taylor's method of expanding series to the term of x^7. Moreover, we measure $-3dB$ bandwidth of $138MHz$. The THD measurements are less than 2.9% for large sinusoid amplitude.

ACKNOWLEDGMENT

The authors would like to thank the National Chip Implementation Center (CIC) of the National Applied Research Laboratories of Taiwan for technical support. The research is supported by the National Science Council of Taiwan, under Grant No. NSC100-2221-E-216-033.

REFERENCES

[1] M. Skrbek, and M. Snorek, "Shift-add neural architecture," Proc. 6th IEE Int. Conference on Circuits and Systems, vol. 1, pp. 411-414, 1999.

[2] S. Marra, M. A. Iachino, and F. C. Morabito, "High speed, programmable implementation of a tanh-like activation function and its derivative for digital neural networks," Proceedings of International Joint Conference on Neural Networks, pp. 506-511, 2007.

[3] M. Carrasco-Robles and L. Serrano, "A novel CMOS current mode fully differential tanh(x) implementation," ISCAS, pp. 21582161, 2008.

[4] Y. Berg, S. Aunet, O. Naess, and M. Hovin, "A novel low-voltage floating-gate CMOS transconductance amplifier with sinh (tanh) shaped output current," The 8th IEEE International Conference on Electronics, Circuits and Systems, vol. 3, pp. 1461-1464, 2001.

[5] C. A. De La Cruz-Blas, A. Lopez-Martin, and A. Carlosena, "1.5-v mos translinear loops with improved dynamic range and their applications to current-mode signal processing," IEEE Trans. Circuit Syst.-II, vol. 50, pp. 918927, 2003.

[6] W. Liu, S. I. Liu, and S. K. Wei, " CMOS differential-mode exponential voltage-to-current converter," Analog Integrated Circuits and Signal Processing, vol. 45, pp. 163168, 2005.

[7] M. Mottaghi kashtiban, A. Khoei, and K. Hadidi, "A current mode, first-order Takagi-Sugeno-Kang fuzzy logic controller, supporting rational-powered membership functions," IEICE Trans. Electron, vol. E90-C, pp. 12581266, 2007.

[8] M. T. Abuelmaatti, "Universal CMOS current-mode analog function synthesizer," IEEE Trans. Circuit Syst.-I, vol. 49, pp. 14681474, 2002.
[9] M. Kumngern, J. Chanwutitum, and K. Dejhan, "Simple CMOS current-mode exponential function generator circuit," Proceedings of ECTI-CON, Krabi, pp. 709712, 2008.
[10] M. Akay, Nonlinear Biomedical Signal Processing, Fuzzy Logic, Neural Networks, and New Algorithms, 2000.
[11] A. Motamed, C. Hwang, and M. Ismail, "CMOS exponential current-to-voltage converter," Electron. Lett., vol. 33, pp. 9981000, 1997.
[12] K. J. Lin, C. J. Cheng, S. F. Chiu, and H. C. Su, "CMOS current-mode implementation of fractional-power functions," Circuits, Systems, and Signal Processing, vol. 31, pp. 61-75, 2012.

國科會補助計畫衍生研發成果推廣資料表

日期:2012/10/27

國科會補助計畫	計畫名稱: 使用多段曲線擬合方法實現CMOS電流模式函數
	計畫主持人: 林國珍
	計畫編號: 100-2221-E-216-033- 學門領域: 積體電路及系統設計

無研發成果推廣資料

100 年度專題研究計畫研究成果彙整表

計畫主持人：林國珍	計畫編號：100-2221-E-216-033-
計畫名稱：使用多段曲線擬合方法實現 CMOS 電流模式函數	

成果項目			量化			單位	備註（質化說明：如數個計畫共同成果、成果列為該期刊之封面故事...等）
			實際已達成數（被接受或已發表）	預期總達成數(含實際已達成數)	本計畫實際貢獻百分比		
國內	論文著作	期刊論文	0	0	100%	篇	
		研究報告/技術報告	0	0	100%		
		研討會論文	0	0	100%		
		專書	0	0	100%		
	專利	申請中件數	0	0	100%	件	
		已獲得件數	0	0	100%		
	技術移轉	件數	0	0	100%	件	
		權利金	0	0	100%	千元	
	參與計畫人力（本國籍）	碩士生	0	0	100%	人次	
		博士生	1	1	100%		
		博士後研究員	0	0	100%		
		專任助理	0	0	100%		
國外	論文著作	期刊論文	1	1	40%	篇	
		研究報告/技術報告	0	0	100%		
		研討會論文	2	2	60%		
		專書	0	0	100%	章/本	
	專利	申請中件數	0	0	100%	件	
		已獲得件數	0	0	100%		
	技術移轉	件數	0	0	100%	件	
		權利金	0	0	100%	千元	
	參與計畫人力（外國籍）	碩士生	0	0	100%	人次	
		博士生	0	0	100%		
		博士後研究員	0	0	100%		
		專任助理	0	0	100%		

其他成果 (無法以量化表達之成果如辦理學術活動、獲得獎項、重要國際合作、研究成果國際影響力及其他協助產業技術發展之具體效益事項等，請以文字敘述填列。)	無

	成果項目	量化	名稱或內容性質簡述
科教處計畫加填項目	測驗工具(含質性與量性)	0	
	課程/模組	0	
	電腦及網路系統或工具	0	
	教材	0	
	舉辦之活動/競賽	0	
	研討會/工作坊	0	
	電子報、網站	0	
	計畫成果推廣之參與（閱聽）人數	0	

國科會補助專題研究計畫成果報告自評表

請就研究內容與原計畫相符程度、達成預期目標情況、研究成果之學術或應用價值（簡要敘述成果所代表之意義、價值、影響或進一步發展之可能性）、是否適合在學術期刊發表或申請專利、主要發現或其他有關價值等，作一綜合評估。

1. 請就研究內容與原計畫相符程度、達成預期目標情況作一綜合評估

■達成目標

□未達成目標（請說明，以 100 字為限）

□實驗失敗

□因故實驗中斷

□其他原因

說明：

2. 研究成果在學術期刊發表或申請專利等情形：

論文：■已發表 □未發表之文稿 □撰寫中 □無

專利：□已獲得 □申請中 ■無

技轉：□已技轉 □洽談中 ■無

其他：(以 100 字為限)

3. 請依學術成就、技術創新、社會影響等方面，評估研究成果之學術或應用價值（簡要敘述成果所代表之意義、價值、影響或進一步發展之可能性）(以 500 字為限)

本研究計畫利用分段趨近的方式，提出實現的電路與趨近的二次多項式電路來達成所要表達的複雜函數電路。所使用的電路特色是電流模式，能更擴大所需要的動態輸入範圍，可貢獻在可變增益放大器的應用上及一些複雜函數的實現，例如應用 Sigmoid 的類神經網路等學術應用。

在分段的技術上，我們採用電流控制的方式來切割段落。然而每個段落的二次多項式電路也必須精準地表現該段落的曲線，因此在控制分段的電路與二次多項式電路及輸入電流大小之間的介面就容易造成偏差，因此我們使用特別設計的定電流模組，將造成偏差的因素，由定電流模組來共同解決。

因為有大的動態輸入範圍，如果應用於手機通訊上的可變增益放大器放大來自基地台的微弱訊號，將可大幅提高手機的收訊品質。另外如果應用於類神經網路，則可將手機帶入更智慧型的領域。當然，更進一步的發展，必須搭配更深入的研究，例如針對特定的精度要求，我們必須分割更多段數來完成，而多少的段數及多大的範圍是電路所不能負擔的，皆需要進一步的研究。對於可變增益放大器的實作上，也要下點功夫，研究適當的演算法來實現較低功率的電路。